PDRs4All: A JWST Early Release Science Program on Radiative Feedback from Massive Stars

Berné, Olivier; Habart, Émilie; Peeters, Els; Abergel, Alain; Bergin, Edwin A.; Bernard-Salas, Jeronimo; Bron, Emeric; Cami, Jan; Dartois, Emmanuel; Fuente, Asunción; ...

Publications of the Astronomical Society of the Pacific, 134:054301 (22pp), 2022 May https://doi.org/10.1088/1538-3873/ac604c

PDRs4All: A JWST Early Release Science Program on Radiative Feedback from Massive Stars

PI Team:
Olivier Berné[1], Émilie Habart[2], Els Peeters[3,4,5]
Core Team:
Alain Abergel[2], Edwin A. Bergin[6], Jeronimo Bernard-Salas[7,8], Emeric Bron[9], Jan Cami[3,4,5], Emmanuel Dartois[10], Asunción Fuente[11], Javier R. Goicoechea[12], Karl D. Gordon[13,14], Yoko Okada[15], Takashi Onaka[16,17], Massimo Robberto[13,18], Markus Röllig[15], Alexander G. G. M. Tielens[19,20], Sílvia Vicente[21], Mark G. Wolfire[20]
Extended Core Team:
Felipe Alarcón[6], C. Boersma[22], Amélie Canin[1], Ryan Chown[3,4], Daniel Dicken[2], David Languignon[9], Romane Le Gal[1,23,24], Marc W. Pound[20], Boris Trahin[2], Thomas Simmer[2], Ameek Sidhu[3,4], Dries Van De Putte[13]
One-time co-authors contributed to SEPs,
Sara Cuadrado[12], Claire Guilloteau[1,25], Alexandros Maragkoudakis[22], Bethany R. Schefter[3], Thiébaut Schirmer[26]
Collaborators:
Stéphanie Cazaux[27], Isabel Aleman[28], Louis Allamandola[22,29], Rebecca Auchettl[30], Giuseppe Antonio Baratta[31], Salma Bejaoui[22], Partha P. Bera[22,29], Goranka Bilalbegović[32], John H. Black[33], Francois Boulanger[34], Jordy Bouwman[35,36,37], Bernhard Brandl[19,38], Philippe Brechignac[10], Sandra Brünken[39], Andrew Burkhardt[40], Alessandra Candian[19,41], Jose Cernicharo[13], Marin Chabot[42], Shubhadip Chakraborty[43], Jason Champion[1], Sean W. J. Colgan[44], Ilsa R. Cooke[45], Audrey Coutens[1], Nick L. J. Cox[46], Karine Demyk[1], Jennifer Donovan Meyer[47], Cécile Engrand[42], Sacha Foschino[1], Pedro García-Lario[48], Lisseth Gavilan[22], Maryvonne Gerin[49], Marie Godard[10], Carl A. Gottlieb[50], Pierre Guillard[51,52], Antoine Gusdorf[34,49], Patrick Hartigan[53], Jinhua He[54,55,56], Eric Herbst[57], Liv Hornekaer[58], Cornelia Jäger[59], Eduardo Janot-Pacheco[60], Christine Joblin[1], Michael Kaufman[61], Francisca Kemper[62,63], Sarah Kendrew[64], Maria S. Kirsanova[65], Pamela Klaassen[66], Collin Knight[3], Sun Kwok[67], Álvaro Labiano[68], Thomas S.-Y. Lai[69], Timothy J. Lee[70], Bertrand Lefloch[23], Franck Le Petit[9], Aigen Li[71], Hendrik Linz[72], Cameron J. Mackie[73,74], Suzanne C. Madden[75], Joëlle Mascetti[76], Brett A. McGuire[77,78], Pablo Merino[79], Elisabetta R. Micelotta[80], Karl Misselt[81], Jon A. Morse[82], Giacomo Mulas[1,83], Naslim Neelamkodan[84,85], Ryou Ohsawa[86], Alain Omont[51], Roberta Paladini[87], Maria Elisabetta Palumbo[31], Amit Pathak[88], Yvonne J. Pendleton[70], Annemieke Petrignani[89], Thomas Pino[10], Elena Puga[90], Naseem Rangwala[44], Mathias Rapacioli[91], Alessandra Ricca[5,22], Julia Roman-Duval[92], Joseph Roser[5,22], Evelyne Roueff[9], Gaël Rouillé[59], Farid Salama[22], Dinalva A. Sales[93], Karin Sandstrom[94], Peter Sarre[95], Ella Sciamma-O'Brien[22], Kris Sellgren[96], Matthew J. Shannon[22], Sachindev S. Shenoy[97], David Teyssier[98], Richard D. Thomas[99], Aditya Togi[100], Laurent Verstraete[2], Adolf N. Witt[101], Alwyn Wootten[47], Nathalie Ysard[2], Henning Zettergren[99], Yong Zhang[102], Ziwei E. Zhang[103], and Junfeng Zhen[104]

[1] Institut de Recherche en Astrophysique et Planétologie, Université de Toulouse, CNRS, CNES, UPS, 9 Av. du colonel Roche, F-31028 Toulouse Cedex 04, France
pis@jwst-ism.org
[2] Institut d'Astrophysique Spatiale, Université Paris-Saclay, CNRS, Bâtiment 121, F-91405 Orsay Cedex, France
[3] Department of Physics & Astronomy, The University of Western Ontario, London ON N6A 3K7, Canada
[4] Institute for Earth and Space Exploration, The University of Western Ontario, London ON N6A 3K7, Canada
[5] Carl Sagan Center, SETI Institute, 339 Bernardo Avenue, Suite 200, Mountain View, CA 94043, USA
[6] Department of Astronomy, University of Michigan, 1085 South University Avenue, Ann Arbor, MI 48109, USA
[7] ACRI-ST, Centre d'Etudes et de Recherche de Grasse (CERGA), 10 Av. Nicolas Copernic, F-06130 Grasse, France
[8] INCLASS Laboratoire Commun., 10 Av. Nicolas Copernic, 06130 Grasse, France
[9] LERMA, Observatoire de Paris, PSL Research University, CNRS, Sorbonne Universités, F-92190 Meudon, France
[10] Institut des Sciences Moléculaires d'Orsay, Université Paris-Saclay, CNRS, Bâtiment 520, F-91405 Orsay Cedex, France
[11] Observatorio Astronómico Nacional (OAN, IGN), Alfonso XII, 3, E-28014 Madrid, Spain
[12] Instituto de Física Fundamental (CSIC), Calle Serrano 121-123, E-28006, Madrid, Spain
[13] Space Telescope Science Institute, 3700 San Martin Drive, Baltimore, MD 21218, USA
[14] Sterrenkundig Observatorium, Universiteit Gent, Gent, Belgium
[15] I. Physikalisches Institut der Universität zu Köln, Zülpicher Straße 77, D-50937 Köln, Germany
[16] Department of Physics, Faculty of Science and Engineering, Meisei University, 2-1-1 Hodokubo, Hino, Tokyo 191-8506, Japan
[17] Department of Astronomy, Graduate School of Science, The University of Tokyo, 7-3-1 Bunkyo-ku, Tokyo 113-0033, Japan
[18] Johns Hopkins University, 3400 N. Charles Street, Baltimore, MD 21218, USA
[19] Leiden Observatory, Leiden University, P.O. Box 9513, 2300 RA Leiden, The Netherlands

[20] Astronomy Department, University of Maryland, College Park, MD 20742, USA
[21] Instituto de Astrofísica e Ciências do Espaço, Tapada da Ajuda, Edifício Leste, 2° Piso, P-1349-018 Lisboa, Portugal
[22] NASA Ames Research Center, MS 245-6, Moffett Field, CA 94035-1000, USA
[23] Institut de Planétologie et d'Astrophysique de Grenoble (IPAG), Université Grenoble Alpes, CNRS, F-38000 Grenoble, France
[24] Institut de Radioastronomie Millimétrique (IRAM), 300 rue de la piscine, F-38406 Saint-Martin d'Hères, France
[25] Institut de Recherche en Informatique de Toulouse, INP-ENSEEIHT, 2 Rue Charles Camichel, F-31071 Toulouse Cedex 07, France
[26] Department of Space, Earth and Environment, Chalmers University of Technology, Onsala Space Observatory, SE-439 92 Onsala, Sweden
[27] Delft University of Technology, Delft, The Netherlands
[28] Instituto de Física e Química, Universidade Federal de Itajubá, Av. BPS 1303, Pinheirinho, 37500-903, Itajubá, MG, Brazil
[29] Bay Area Environmental Research Institute, Moffett Field, CA 94035, USA
[30] Australian Synchrotron, Australian Nuclear Science and Technology Organisation (ANSTO), Victoria, Australia
[31] INAF—Osservatorio Astrofisico di Catania, Via Santa Sofia 78, I-95123 Catania, Italy
[32] Department of Physics, Faculty of Science, University of Zagreb, Bijenička cesta 32, 10000 Zagreb, Croatia
[33] Department of Space, Earth, and Environment, Chalmers University of Technology, Onsala Space Observatory, SE-43992 Onsala, Sweden
[34] Laboratoire de Physique de l'École Normale Supérieure, ENS, Université PSL, CNRS, Sorbonne Université, Université de Paris, F-75005, Paris, France
[35] Laboratory for Atmospheric and Space Physics, University of Colorado, Boulder, CO 80303, USA
[36] Department of Chemistry, University of Colorado, Boulder, CO 80309, USA
[37] Institute for Modeling Plasma, Atmospheres, and Cosmic Dust (IMPACT), University of Colorado, Boulder, CO 80303, USA
[38] Faculty of Aerospace Engineering, Delft University of Technology, Kluyverweg 1, 2629 HS Delft, The Netherlands
[39] Radboud University, Institute for Molecules and Materials, FELIX Laboratory, Toernooiveld 7, 6525 ED Nijmegen, the Netherlands
[40] Department of Physics, Wellesley College, 106 Central Street, Wellesley, MA 02481, USA
[41] TU Library, Delft University of Technology, Prometheusplein 1, 2628 ZC Delft, The Netherlands
[42] Laboratoire de Physique des deux infinis Irène Joliot-Curie, Université Paris-Saclay, CNRS/IN2P3, Bâtiment 104, F-91405 Orsay Cedex, France
[43] Institut de Physique de Rennes, UMR CNRS 6251, Université de Rennes 1, Campus de Beaulieu, F-35042 Rennes Cedex, France
[44] NASA Ames Research Center, Moffett Field, CA 94035, USA
[45] Department of Chemistry, The University of British Columbia, Vancouver, British Columbia, Canada
[46] ACRI-ST, 260 route du Pin Montard, F-06904, Sophia Antipolis, France
[47] National Radio Astronomy Observatory (NRAO), 520 Edgemont Road, Charlottesville, VA 22903, USA
[48] European Space Astronomy Centre (ESAC/ESA), Villanueva de la Cañada, E-28692 Madrid, Spain
[49] Observatoire de Paris, PSL University, Sorbonne Université, LERMA, F-75014, Paris, France
[50] Harvard-Smithsonian Center for Astrophysics, 60 Garden Street, Cambridge MA 02138, USA
[51] Sorbonne Université, CNRS, UMR 7095, Institut d'Astrophysique de Paris, 98bis bd Arago, F-75014 Paris, France
[52] Institut Universitaire de France, Ministère de l'Enseignement Supérieur et de la Recherche, 1 rue Descartes, F-75231 Paris Cedex 05, France
[53] Department of Physics and Astronomy, Rice University, Houston, TX 77005-1892, USA
[54] Yunnan Observatories, Chinese Academy of Sciences, 396 Yangfangwang, Guandu District, Kunming, 650216, People's Republic of China
[55] Chinese Academy of Sciences South America Center for Astronomy, National Astronomical Observatories, CAS, Beijing 100101, People's Republic of China
[56] Departamento de Astronomía, Universidad de Chile, Casilla 36-D, Santiago, Chile
[57] Departments of Chemistry and Astronomy, University of Virginia, Charlottesville, VA 22904, USA
[58] InterCat and Dept. Physics and Astron., Aarhus University, Ny Munkegade 120, DK-8000 Aarhus C, Denmark
[59] Laboratory Astrophysics Group of the Max Planck Institute for Astronomy at the Friedrich Schiller University Jena, Institute of Solid State Physics, Helmholtzweg 3, D-07743 Jena, Germany
[60] Instituto de Astronomia, Geofísica e Ciências Atmosféricas, Universidade de São Paulo, 05509-090 São Paulo, SP, Brazil
[61] Department of Physics and Astronomy, San José State University, San Jose, CA 95192, USA
[62] European Southern Observatory, Karl-Schwarzschild-Str. 2, D-85748 Garching b. München, Germany
[63] Institute of Astronomy and Astrophysics, Academia Sinica, No. 1, Sec. 4, Roosevelt Rd., Taipei 10617, Taiwan
[64] European Space Agency, Space Telescope Science Institute, 3700 San Martin Drive, Baltimore, MD 21218, USA
[65] Institute of Astronomy, Russian Academy of Sciences, 119017, Pyatnitskaya str., 48 , Moscow, Russia
[66] UK Astronomy Technology Centre, Royal Observatory Edinburgh, Blackford Hill EH9 3HJ, UK
[67] Department of Earth, Ocean, & Atmospheric Sciences, University of British Columbia, V6T 1Z4, Canada
[68] Telespazio UK for ESA, ESAC, E-28692 Villanueva de la Cañada, Madrid, Spain
[69] IPAC, California Institute of Technology, Pasadena, CA, USA
[70] NASA Ames Research Center, MS 245-3, Moffett Field, CA 94035-1000, USA
[71] Department of Physics and Astronomy, University of Missouri, Columbia, MO 65211, USA
[72] Max Planck Institute for Astronomy, Königstuhl 17, D-69117 Heidelberg, Germany
[73] Chemical Sciences Division, Lawrence Berkeley National Laboratory, Berkeley, CA, USA
[74] Kenneth S. Pitzer Center for Theoretical Chemistry, Department of Chemistry, University of California—Berkeley, Berkeley, CA, USA
[75] AIM, CEA, CNRS, Université Paris-Saclay, Université Paris Diderot, Sorbonne Paris Cité, F-91191 Gif-sur-Yvette, France
[76] Institut des Sciences Moléculaires, CNRS, Université de Bordeaux, F-33405 Talence, France
[77] Department of Chemistry, Massachusetts Institute of Technology, Cambridge, MA 02139, USA
[78] National Radio Astronomy Observatory, Charlottesville, VA 22903, USA
[79] Instituto de Ciencia de Materiales de Madrid (CSIC), Sor Juana Ines de la Cruz 3, E-28049, Madrid, Spain
[80] Department of Physics, P.O. Box 64, FI-00014 University of Helsinki, Finland
[81] Steward Observatory, University of Arizona, Tucson, AZ 85721-0065, USA
[82] BoldlyGo Institute, 31 W 34TH ST FL 7 STE 7159, New York, NY 10001, USA
[83] INAF—Osservatorio Astronomico di Cagliari, via della scienza 5, I-09047 Selargius, Italy
[84] Department of Physics, College of Science, United Arab Emirates University (UAEU), Al-Ain, 15551, UAE
[85] National Astronomical Observatory of Japan, National Institutes of Natural Science, 2-21-1 Osawa, Mitaka, Tokyo 181-8588, Japan
[86] Institute of Astronomy, Graduate School of Science, The University of Tokyo, 2-21-1, Osawa, Mitaka, Tokyo 181-0015, Japan
[87] California Institute of Technology, IPAC, 770, S. Wilson Ave., Pasadena, CA 91125, USA
[88] Department of Physics, Institute of Science, Banaras Hindu University, Varanasi 221005, India

[89] Van't Hoff Institute for Molecular Sciences, University of Amsterdam, P.O. Box 94157, 1090 GD, Amsterdam, The Netherlands
[90] European Space Agency (ESA), ESA Office, Space Telescope Science Institute, 3700 San Martin Drive, Baltimore, MD 21218, USA
[91] Laboratoire de Chimie et Physique Quantiques LCPQ/IRSAMC, UMR5626, Université de Toulouse (UPS) and CNRS, Toulouse, France
[92] Space Telescope Science Institute, 3700 San Martin Drive, Baltimore, MD 21218, USA
[93] Instituto de Matemática, Estatística e Física, Universidade Federal do Rio Grande, 96201-900, Rio Grande, RS, Brazil
[94] Center for Astrophysics and Space Sciences, Department of Physics, University of California, San Diego, 9500 Gilman Drive, La Jolla, CA 92093, USA
[95] School of Chemistry, The University of Nottingham, University Park, Nottingham, NG7 2RD, UK
[96] Astronomy Department, Ohio State University, Columbus, OH 43210, USA
[97] Space Science Institute, 4765 Walnut St., R203, Boulder, CO 80301, USA
[98] Telespazio Vega UK Ltd for European Space Agency (ESA), Camino bajo del Castillo, s/n, Urbanizacion Villafranca del Castillo, Villanueva de la Cañada, E-28692 Madrid, Spain
[99] Department of Physics, Stockholm University, SE-10691 Stockholm, Sweden
[100] Department of Physics, Texas State University, San Marcos, TX 78666, USA
[101] Ritter Astrophysical Research Center, University of Toledo, Toledo, OH 43606, USA
[102] School of Physics and Astronomy, Sun Yat-sen University, 2 Da Xue Road, Tangjia, Zhuhai 519000, Guangdong Province, People's Republic of China
[103] Star and Planet Formation Laboratory, RIKEN Cluster for Pioneering Research, Wako, Saitama 351-0198, Japan
[104] University of Science and Technology of China, CAS Key Laboratory of Crust-Mantle Materials and Environment, Hefei, Anhui 230026, People's Republic of China
Received 2022 January 13; accepted 2022 March 23; published 2022 June 1

Abstract

Massive stars disrupt their natal molecular cloud material through radiative and mechanical feedback processes. These processes have profound effects on the evolution of interstellar matter in our Galaxy and throughout the universe, from the era of vigorous star formation at redshifts of 1–3 to the present day. The dominant feedback processes can be probed by observations of the Photo-Dissociation Regions (PDRs) where the far-ultraviolet photons of massive stars create warm regions of gas and dust in the neutral atomic and molecular gas. PDR emission provides a unique tool to study in detail the physical and chemical processes that are relevant for most of the mass in inter- and circumstellar media including diffuse clouds, proto-planetary disks, and molecular cloud surfaces, globules, planetary nebulae, and star-forming regions. PDR emission dominates the infrared (IR) spectra of star-forming galaxies. Most of the Galactic and extragalactic observations obtained with the James Webb Space Telescope (JWST) will therefore arise in PDR emission. In this paper we present an Early Release Science program using the MIRI, NIRSpec, and NIRCam instruments dedicated to the observations of an emblematic and nearby PDR: the Orion Bar. These early JWST observations will provide template data sets designed to identify key PDR characteristics in JWST observations. These data will serve to benchmark PDR models and extend them into the JWST era. We also present the Science-Enabling products that we will provide to the community. These template data sets and Science-Enabling products will guide the preparation of future proposals on star-forming regions in our Galaxy and beyond and will facilitate data analysis and interpretation of forthcoming JWST observations.

Unified Astronomy Thesaurus concepts: Photodissociation regions (1223); Infrared telescopes (794); Polycyclic aromatic hydrocarbons (1280); Star forming regions (1565); Gaseous nebulae (639)

1. Introduction

The James Webb Space Telescope (JWST, Gardner et al. 2006) is a 6.5 m space telescope launched in 2021 December and is developed by the National Aeronautics and Space Administration (NASA), the European Space Agency (ESA), and the Canadian Space Agency (CSA). Following recommendations of the science advisory board of the JWST, the Space Telescope Science Institute (STScI), in charge of the scientific operations of the JWST, issued a call for "Early Release Science[105]," (ERS) programs. The goals of these programs are (1) to provide first-look public data to the astronomical community as soon as possible after launch, (2) to further test the instruments and observing modes in addition to tests performed during commissioning and showcase the technical capabilities of JWST, and (3) to help prepare the community for General Observers (GO) proposals. An important aspect of ERS programs is that they must deliver highly processed data quickly (within 3–5 months of observations) and provide Science-Enabling Products (SEPs) to the community.

In this paper, we present one of the 13 accepted ERS programs called "PDRs4All: Radiative feedback from massive stars" (ID1288)[106] which is dedicated to studying the interactions of massive stars with their surroundings. We first describe the general scientific context in Section 2. We then describe the immediate objectives of this program in Section 3 and its science objectives in Section 5. We discuss the target, the Orion Bar, in Section 4 and describe simulated infrared (IR)

[105] https://jwst.stsci.edu/science-planning/calls-for-proposals-and-policy/early-release-science-program

[106] pdrs4all.org; https://www.stsci.edu/jwst/science-execution/program-information.html?id=1288

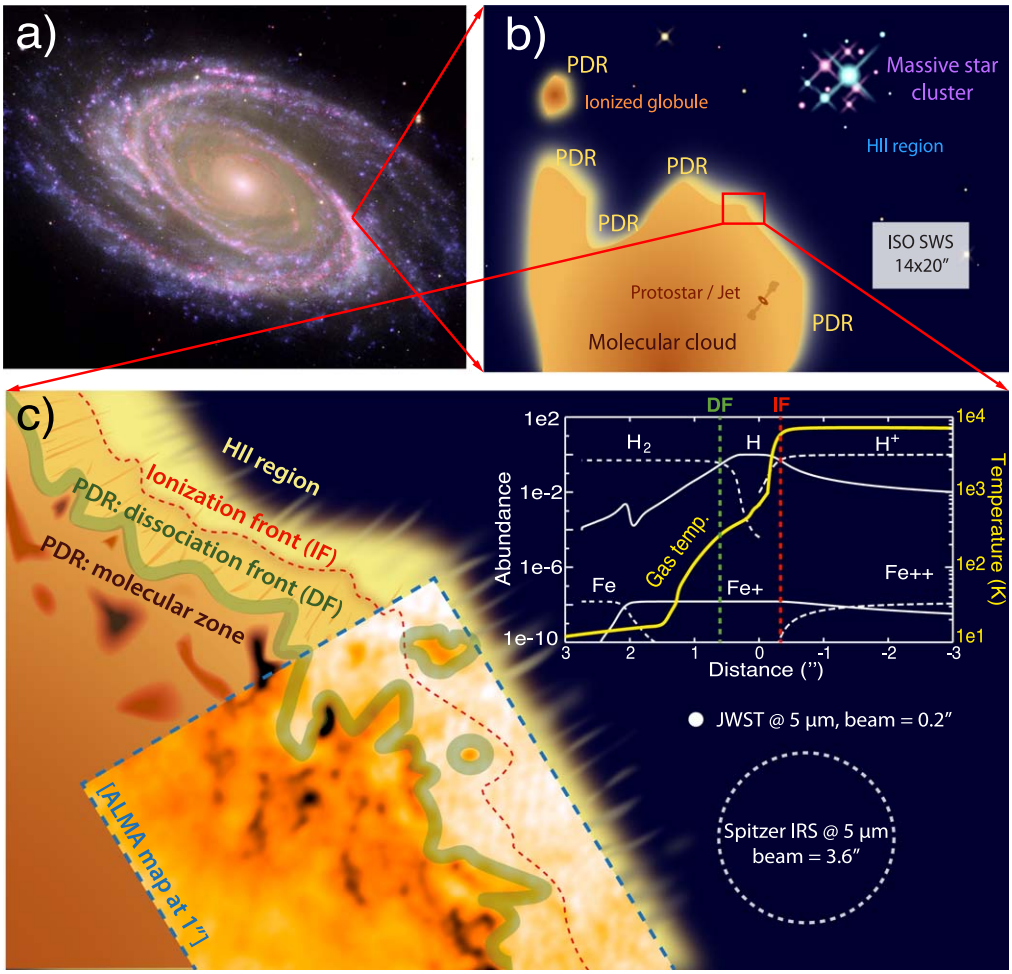

Figure 1. Zooming into a PDR. (a) Multi-wavelength view of a galaxy (M81): UV-tracing massive stars (blue), optical-light-tracing H II regions (green), and emission in the Aromatic Infrared Bands (AIBs) tracing PDRs (red). Credits: Hubble data: NASA, ESA, and A. Zezas (Harvard-Smithsonian Center for Astrophysics); GALEX data: NASA, JPL-Caltech, GALEX Team, J. Huchra et al. (Harvard-Smithsonian Center for Astrophysics); Spitzer data: NASA/JPL/Caltech/S. Willner (Harvard-Smithsonian Center for Astrophysics). (b) Sketch of a typical massive star-forming region. (c) Zoom in on the PDR, showing the complex transition from the molecular cloud to the PDR dissociation front, the ionization front and the ionized gas flow. Inserted is the ALMA molecular gas data of the Orion Bar, at a resolution of 1″ (dashed lines; Goicoechea et al. 2016). The plot shows a model of the structure of the PDR. The scale length for FUV photon penetration corresponds to a few arcsec. The beam sizes of ISO-SWS, Spitzer-IRS, and JWST-MIRI are indicated. JWST will resolve the 4 key regions: the molecular zone, the H_2 dissociation front, the ionization front, and the fully ionized flow into the H II region (see Section 2.1).

spectra for this source in Section 6. The planned observations are presented in Section 7. Section 8 gives an overview of the SEPs developed for this program. We briefly present the team in Section 9 and conclude in Section 10.

2. Importance of PDRs in the JWST Era

2.1. Photo-dissociation Regions

Photo-Dissociation Regions (PDRs; Figure 1) are regions near massive stars, where most of the gas is neutral (i.e., H or H_2) and is heated by far-ultraviolet (FUV) photons (i.e., $6\,\mathrm{eV} < E < 13.6\,\mathrm{eV}$). Four key zones can be identified across the PDR: the *molecular zone*, where the gas is nearly fully molecular, dense, and cold (several tens of K); the H_2 dissociation front (DF), where the gas converts from nearly fully molecular to atomic and the temperature rises from 30 to 300 K; the ionization front (IF) where the gas converts from fully neutral to fully ionized and the temperature increases to 7000 K; and the fully ionized flow into the H II region. PDRs have a gas density (n_H for the hydrogen nucleus density) ranging from $n_\mathrm{H} \sim 10^3\,\mathrm{cm}^{-3}$ in diffuse gas to $n_\mathrm{H} \sim 10^6\,\mathrm{cm}^{-3}$ in dense star-forming regions. The incident flux of the FUV field on the PDRs, G_0, is commonly characterized in units of the Habing field corresponding to $1.6 \times 10^{-3}\,\mathrm{erg\,s^{-1}\,cm^{-2}}$ when

integrated between 6 and 13.6 eV (Habing 1968). The standard interstellar radiation field has a G_0 value of ~1.7 (Draine 1978; Parravano et al. 2003) while in most PDRs, G_0 is higher and can go up to a few 10^5. The kinetic temperature of the gas (T_g) in PDRs lies between ten and a few thousand degrees. Large dust grains (0.1 μm and above) are in equilibrium with the radiation field at temperatures of ~30–70 K (e.g., Anderson et al. 2012; Paladini et al. 2012). Highly irradiated PDRs can be found surrounding young H II regions formed by O and early B stars (Sternberg & Dalgarno 1989). At the ionized front, the gas is compressed by the expansion of the ionized gas, the FUV radiation field is high ($G_0 = 10^{4-5}$), and densities and temperatures are also high ($n_H \sim 10^{5-6}$ cm^{-3} and $T_g \sim 100$ to 2000 K). These are the physical conditions found in one of the most studied PDRs, the Orion Bar (see e.g., Tielens & Hollenbach 1985a; Goicoechea et al. 2016). Around less massive B stars, or at the interfaces of more evolved H II regions, PDRs have a lower FUV radiation field ($G_0 = 10^{2-4}$) as observed for instance in PDRs like NGC 2023 (Burton et al. 1998; Sheffer et al. 2011), NGC 7023 (Fuente et al. 2003), or the Horsehead nebula (Habart et al. 2011; Pabst et al. 2017). The diffuse medium in the Milky Way is a vast, low density ($n_H \sim 10$ cm^{-3}) and low FUV radiation field ($G_0 = 1-10$) PDR (van Dishoeck & Black 1986), where the temperature is of the order of 50–100 K (Wolfire et al. 2003).

Inside PDRs, the gas is mainly heated by the photoelectric effect working on Polycyclic Aromatic Hydrocarbon (PAH) molecules and small dust grains (Verstraete et al. 1990; Bakes & Tielens 1994; Weingartner & Draine 2001). Deep in the PDR, where the FUV radiation field is attenuated due to dust absorption in the outer layers, collisions of the gas with warm dust grains and cosmic-ray heating become important (e.g., Tielens 2005). Other heating mechanisms through H_2 formation or UV pumping of H_2 followed by de-excitation may provide additional important heating sources near the edge of dense PDRs (e.g., Le Petit et al. 2006; Le Bourlot et al. 2012). The gas in PDRs is mostly cooled by far-IR (FIR) fine-structure lines, such as the [C II] line at 158 μm and the [O I] lines at 63 and 146 μm (e.g., Hollenbach & Tielens 1999; Bernard-Salas et al. 2012). The interplay between heating and cooling mechanisms results in a large temperature gradient from the ionized to molecular gas across the PDR (Figure 1(c)).

Models have been very successful in explaining large-scale Galactic and extra-galactic observations of PDRs (e.g., Tielens & Hollenbach 1985b; Sternberg & Dalgarno 1989; Wolfire et al. 1990; Abgrall et al. 1992; Le Bourlot et al. 1993; Kaufman et al. 2006; Röllig et al. 2007; Cubick et al. 2008). However, Atacama Large Millimeter/submillimeter Array (ALMA) observations unambiguously revealed a highly sculpted interface between the molecular clouds and the ionized gas (Figure 1; Goicoechea et al. 2016) and have challenged the traditional "layered structure" view of PDRs (and their models). Moreover, recent near-IR images obtained with the Gemini or Keck telescopes at high spatial resolution (~0.″1), similar to JWST, revealed with a spectacular level of detail structures unexpected within the classic irradiated molecular cloud (e.g., Hartigan et al. 2020; E. Habart et al. 2022, in preparation). A series of ridges that follow along the interfaces may be associated with a multitude of small dense highly irradiated PDRs. JWST will resolve and observe directly the response of the gas to the penetrating FUV photons and give for the first time insight into the physical conditions and chemical composition of this very structured irradiated medium.

2.2. PDRs Everywhere

Stars in galaxies only form in cold gas, hence the efficiency at which the energy of FUV photons from massive stars is transferred to the interstellar gas in PDRs has a critical impact on the star formation rate. This efficiency can typically be monitored using the mid-IR emission of nearby and distant galaxies (e.g., Helou et al. 2001; Peeters et al. 2004b; Maragkoudakis et al. 2018; Calzetti 2020; McKinney et al. 2020). Mid-IR observations are also useful to disentangle the contribution of shock versus PDR gas heating in galaxies (e.g., merger versus starburst van den Ancker et al. 2000; Guillard et al. 2012). Dense ($n_H > 10^4$ cm^{-3}) and highly irradiated ($G_0 \sim 10^{4-6}$) PDRs are also present in the FUV-illuminated surfaces of protoplanetary disks (e.g., Visser et al. 2007; Woitke et al. 2009) and govern the mass loss of these objects through photoevaporation (Gorti et al. 2009) in competition with planet formation. IR observations give direct diagnostics of the FUV energy injected into the gas (e.g., Meeus et al. 2013) and, in combination with PDR models, can constrain the physical parameters (T_g, n_H) inside the FUV-driven winds of these disks (e.g., Champion et al. 2017). Observations and models of planetary nebulae show that a large fraction of the gas ejected by evolved stars goes through a PDR phase (Hollenbach & Natta 1995; Bernard-Salas & Tielens 2005) before being injected into the interstellar medium (ISM). Here again, IR spectroscopy provides key information on the initial physical and chemical properties of the material in this phase (e.g., Bernard-Salas et al. 2009; Cox et al. 2015) and allows the photochemical evolution of molecules, nanoparticles, and grains to be probed. Clearly, PDRs are present in a wide variety of environments.

2.3. IR Signatures of PDRs

PDRs emit mainly in the IR. Key PDR signatures in the near- and mid-IR (1–28 μm) include (i) the Aromatic Infrared Bands (AIBs, Figure 2), attributed to Polycyclic Aromatic Hydrocarbons (PAHs) and related species that are heated by absorption of UV photons (Leger & Puget 1984; Allamandola et al. 1985), (ii) continuum emission, attributed to very small carbonaceous grains (VSGs, Désert et al. 1990), (iii)

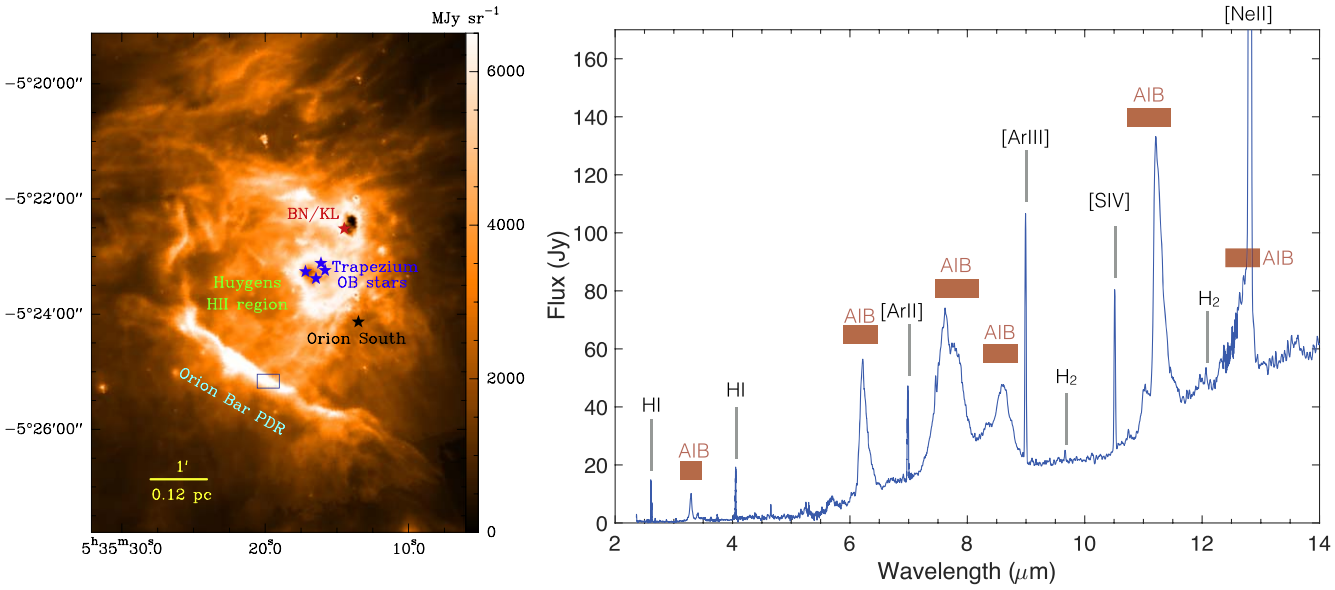

Figure 2. The Orion Bar in the mid-IR. Left: Overview of the central region of the Orion Nebula as seen with Spitzer-IRAC at 8 μm. Salient objects, including the Orion Bar which is the target of this program, are labeled. Figure adapted from Goicoechea et al. (2015). Right: ISO-SWS spectrum of the Orion Bar PDR extracted at the position indicated by the blue box in the image (for the 2.3–12 μm range). Main spectroscopic fingerprints are labeled.

rovibrational and pure rotational lines of H_2 (Rosenthal et al. 2000), and (iv) emission lines from atomic ions (e.g., S^+, Si^+, Fe^+, Kaufman et al. 2006), and (v), in regions close to massive stars, emission from larger grains composed of silicates (Draine 2003) or a mixture of silicates and carbonaceous material at thermal equilibrium (Draine & Li 2007; Jones et al. 2013).

A large fraction of the observations that will be obtained with JWST will correspond to emission that is forged inside PDRs. It is therefore of paramount importance to understand how the observed mid-IR emission fingerprints are linked with physical conditions, and how these observations can be turned into probes of astrophysical environments. This requires detailed knowledge of how PDRs "work," by observing nearby, extended PDRs. This ERS program is designed to characterize the IR signatures of the Orion Bar PDR, unravel the underlying physical and chemical processes, and validate diagnostic tools in order to facilitate the interpretation of PDR emission to be seen with JWST, in the local and distant universe.

3. Immediate Goals of this ERS Program

The main goal of our program is to rapidly deliver "template data," as well as data processing and analysis tools for PDRs, which will be crucial for JWST proposal preparation for both Galactic and extra-galactic sciences communities. To reach this ambitious goal, we have identified the following three immediate objectives:

1. Characterize the *full* 1–28 μm emission spectrum of the key zones and sub-regions within the ionized gas, the PDR, and the surrounding molecular cloud and determine the physical and chemical conditions in these specific environments.
2. Examine the efficacy and limitations of the narrow/broad band filters in the study of PDRs by accurately calibrating narrow/broad band filters which capture gas lines and AIBs as PDR probes.
3. Deliver tools facilitating post-pipeline data reduction and processing, as well as PDR and AIB analysis tools required for the interpretation of (un)resolved PDR emission to be observed with JWST.

To this end, we will observe the Orion Bar, a proto-typical PDR situated in the Orion Nebula (Figure 2) using NIRCam, NIRSpec, and MIRI in the 1–28 μm wavelength range. The Orion Bar has a well-defined UV illumination and geometry making it an ideal target to reach our science goals. These observations will, for the first time, spatially resolve and perform tomography of the PDR, revealing the individual IR spectral signatures in the four key zones of a PDR: the molecular zone, the H_2 dissociation front, the ionization front, and the ionized flow into the H II region (Figure 1).

4. Target: The Orion Bar

Orion Bar (Figure 2) is a prototype of a strongly UV-irradiated PDR with a nearly edge-on geometry (e.g., Hogerheijde et al. 1995), convenient to study and spatially

resolve the structure, physical conditions, and chemical stratification of a PDR. The Orion Bar is a bright (at many wavelengths, Figure 3) escarpment of the Orion molecular cloud (OMC), the closest[107] site of ongoing massive star formation. The Orion Bar is illuminated by the O7-type star θ^1 Ori C, the most massive member of the Trapezium young stellar cluster, which lies at the heart of the Orion Nebula (about 2′ north west of the Bar, e.g., O'Dell 2001). The intense ionizing radiation and strong winds from θ^1 Ori C power and shape the nebula (Güdel et al. 2008; Pabst et al. 2019) The Bar (also referred to as the Bright Bar (e.g., Balick et al. 1974; Fazio et al. 1974; Werner et al. 1976) historically refers to the elongated rim near the ionization front (originally detected in the radio continuum and in optical lines) that separates the neutral cloud from the ionized H II gas with an electron temperature $T_e \approx 10^4$ K and electron density n_e of several 1000 cm^{-3} (e.g., Weilbacher et al. 2015, and references therein). The UV radiation field incident on the Orion Bar PDR is $G_0 = (1–4) \times 10^4$ (e.g., Marconi et al. 1998). Beyond the ionization front, only FUV photons with energies below 13.6 eV penetrate the cloud. The first PDR layers are predominantly neutral and *atomic*: $[H] > [H_2] \gg [H^+]$. A plethora of NIR lines are emitted from this region (e.g., CI recombination lines, O I fluorescent lines, see Walmsley et al. 2000). This warm and moderately dense gas (n_H of a few 10^4 cm^{-3}) is mainly heated by photoelectrons ejected from PAHs and grains and it is mainly cooled by the FIR [C II] 158 μm and [O I] 63 μm and 145 μm fine-structure lines (e.g., Tielens et al. 1993; Herrmann et al. 1997; Bernard-Salas et al. 2012; Ossenkopf et al. 2013). The observed narrow ($\Delta v = 2–3$ km s^{-1}) carbon and sulfur radio recombination lines also arise from these layers and provide a measure of the electron density in the PDR ($n_e \simeq 10–100$ cm^{-3}; e.g., Wyrowski et al. 1997; Cuadrado et al. 2019; Goicoechea & Cuadrado 2021). The atomic PDR zone also hosts the peak of the MIR AIBs (e.g., Bregman et al. 1989; Sellgren et al. 1990; Tielens et al. 1993; Giard et al. 1994; Knight et al. 2021).

At about 15″ from the ionization front (at $A_V \simeq 1–2$ mag of visual extinction into the neutral cloud), the FUV dissociating photons are sufficiently attenuated and most of the hydrogen becomes molecular, H_2 molecules contain over 90% of the H nuclei (van der Werf et al. 2013). This H/H_2 transition zone (dissociation front) displays a forest of near- and mid-IR rotational and vibrationally excited H_2 lines (e.g., Parmar et al. 1991; Luhman et al. 1994; van der Werf et al. 1996; Allers et al. 2005; Shaw et al. 2009; Zhang et al. 2021), including FUV-pumped vibrational levels up to $v = 10$ (Kaplan et al. 2017) and HD rotational lines (Wright et al. 1999; Joblin et al. 2018). Analysis of the IR H_2 and 21 cm H I lines toward the dissociation front suggests warm kinetic temperatures for the molecular gas ($T_g = 400–700$ K) which are not easy to reproduce by PDR models using standard (diffuse ISM) grain properties and heating rates (e.g., Allers et al. 2005).

Beyond the dissociation front, between $A_V = 1–2$ and 4 mag, the C^+/C/CO transition takes place (e.g., Tauber et al. 1995) and the PDR becomes *molecular*, with the abundance of reactive molecular ions quickly rising (e.g., Stoerzer et al. 1995; Fuente et al. 2003; Nagy et al. 2013; van der Tak et al. 2013). FIR and MIR photometric images reveal that the thermal dust emission peaks deeper into the PDR than the AIBs. They show a dust temperature gradient from $T_d \simeq 70$ K near the ionization front to $T_d \simeq 35$ K in the less exposed layers (Arab et al. 2012; Salgado et al. 2016). Dust models of the Orion Bar require FUV and IR grain opacities lower than in the diffuse ISM, with $R_V = A_V/E_{B-V} \simeq 5.5$, consistent with a flatter extinction curve (e.g., Cardelli et al. 1989; Abel et al. 2006), and with larger-than-standard-size grains.

As the FUV flux drops, T_g and T_d decrease too. The intermediate A_V layers of the Orion Bar PDR show a rich chemical composition which includes a large variety of small hydrocarbons, complex organic species, and some deuterated molecules (e.g., Hogerheijde et al. 1995; Simon et al. 1997; Peeters et al. 2004a; Leurini et al. 2006; Onaka et al. 2014; Cuadrado et al. 2015, 2017; Doney et al. 2016). At greater A_V, as T_d decreases, abundant elements such as oxygen and sulfur atoms start to deplete on dust grains, and ices form. The ice mantle composition and the chemistry that takes place on PDR grain surfaces are still uncertain (e.g., Guzmán et al. 2011; Esplugues et al. 2016). Photodesorption of these ices enriches the gas with new chemical species (e.g., Putaud et al. 2019; Goicoechea et al. 2021, and references therein).

Unfortunately, most of the observations described above (especially at FIR and longer wavelengths) refer to modest angular resolution observations (10″–20″) that do not spatially resolve the main transition zones of the PDR. As a consequence, their fundamental structures: homogeneous versus clumpy, constant density versus constant pressure, and the role of magnetic pressures and dynamical effects (e.g., photoevaporation or low-velocity shocks) are still debated. This ongoing discussion has led to the development of very detailed PDR models (e.,g. Tielens & Hollenbach 1985b; Burton et al. 1990; Störzer & Hollenbach 1998; Pellegrini et al. 2009; Andree-Labsch et al. 2017; Bron et al. 2018; Kirsanova & Wiebe 2019). One of the controversial points is the need to invoke the presence of high-density clumps ($n_H = 10^6–10^7$cm^{-3}) to explain the emission from certain high critical density tracers (e.g., Tauber et al. 1994; van der Werf et al. 1996; Young Owl et al. 2000; Lis & Schilke 2003). Interestingly, the most massive clumps might collapse and form low-mass stars (e.g., Lis & Schilke 2003). However, very small dense clumps may not exist, at least close to the dissociation front (e.g., Gorti & Hollenbach 2002).

[107] The most commonly adopted distance to the Bar is 414 pc (Menten et al. 2007) although more recent observations, including Gaia, point to slightly lower values (Kounkel et al. 2017; Großschedl et al. 2018).

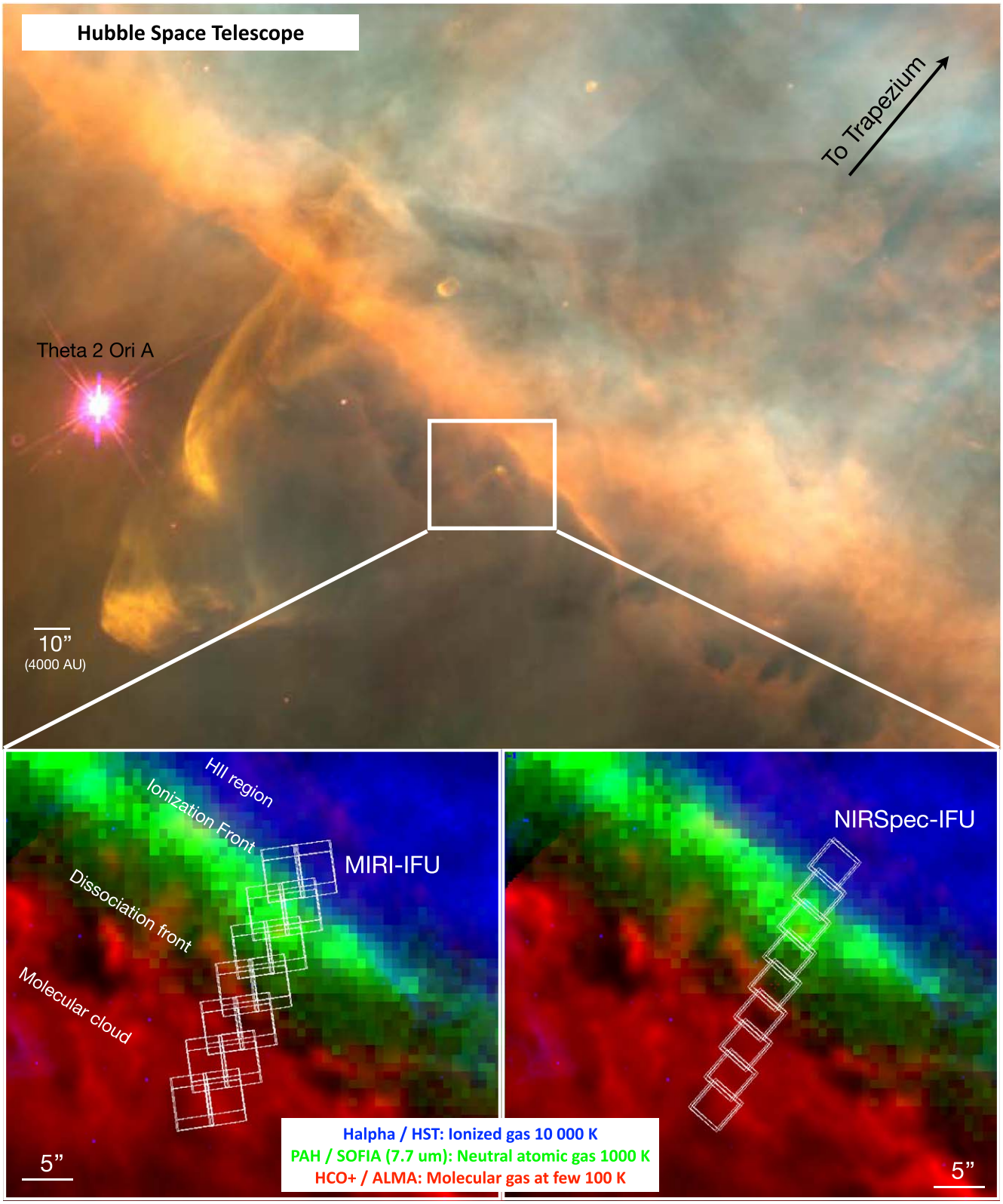

Figure 3. Overview of the Orion Bar region at visible wavelengths, observed with the Hubble Space Telescope (top panel; credits: NASA, C.R. O'Dell and S.K. Wong, Rice University). Lower panels zoom on the region of interest showing the footprints of the MIRI-IFU and NIRSpec-IFU mosaics on a multi-wavelength view of the Orion Bar composed of Hα 656 nm emission (blue, Bally et al. 2000), PAH 7.7 μm emission (green, Salgado et al. 2016), and HCO^+ (4-3) 356.7 GHz emission (red, Goicoechea et al. 2016).

Alternatively, some of the observed features may be explained without invoking clumps by a roughly isobaric PDR, at high thermal pressure ($P_{\rm th}/k \approx 10^8$ cm^{-3} K) (e.g., Allers et al. 2005; Joblin et al. 2018) embedded in a more diffuse medium. In addition, magnetic pressure may play a role in the PDR/clump dynamics (e.g., Pellegrini et al. 2009; Pabst et al. 2020). Recent observations of the FIR dust polarization suggest a plane-of-the-sky magnetic field strength of $B_0 \simeq 300\,\mu$G (Chuss et al. 2019; Guerra et al. 2021).

Recently, ALMA observed the same FOV that JWST will target, providing $\sim$1″ resolution images of the CO and HCO^+ emission (Goicoechea et al. 2016). Instead of a homogeneous PDR with well-defined and spatially separated H/H_2 and C^+/C/CO transition zones, ALMA revealed rich small-scale structures (akin to filaments and globules), sharp edges, and uncovered the presence of an embedded proplyd (object 203–506; Champion et al. 2017). The CO gas temperature just beyond the dissociation front is $T_{\rm k} \simeq 200$ K (see also Habart et al. 2010; Joblin et al. 2018) and decreases deeper inside.

5. Scientific Objectives

The data set that we will obtain with Webb (see Section 7) will allow us to address several science questions. In this section we highlight three science objectives that can be tackled with this ERS program.

Evolution of the physical and chemical conditions at the critical $H^+/H^0/H_2$ transition zones—We expect to detect and spatially resolve a large number of lines (see Section 6 and Figure 6), i.e., fine-structure lines of several ions and atoms (e.g., [Fe II], [Fe I], [Ar III], [Ar II], [S IV], [S II], [S I], [P III], [Ne III], [Ne II], [Ni II], [F I], [Cl I], ...), fluorescent lines (O, N), recombination lines (H, He, C), pure rotational and rovibrational transitions of H_2 and its isotopologue HD (both collisionally excited or radiatively pumped), rovibrational transitions of non-polar molecules (CH_4, C_2H_2, CO_2, C_6H_6), and possibly, for the first time in a PDR, highly excited pure rotational and rovibrational transitions of CO, H_2O (HDO), and OH. Observations of these species, each of which provides a diagnostic of a specific physical environment or chemical reaction, at unprecedented high spatial resolution (up to 0.″1 or 40 au at 400 pc) for a PDR have so far been out of reach.

Variations in the physical conditions and the high-density sub-structures in the critical $H^+/H^0/H_2$ transition zones are poorly known, yet they are of fundamental importance for PDR models and data interpretation. The measurement of a large number of fine-structure lines of ions and atoms will give access to the warm plasma cooling and pressure gradients before the ionization front and between the ionization front and dissociation front (Osterbrock & Ferland 2006). Strong constraints can then be placed on metallicities, electron densities, and temperature variations (e.g., Figure 4(b) and Verma et al. 2003). Benchmarking these probes of ionized/neutral gas interface is particularly important to support extragalactic studies (e.g., Cormier et al. 2012). A description of the impinging UV radiation field (intensity and wavelength dependence) can also be obtained via fluorescent lines (e.g., Walmsley et al. 2000). A determination of the physical conditions in the neutral layer beyond the ionization front can also be assessed with recombination lines (e.g., Natta et al. 1994; Cuadrado et al. 2019). On the other hand, pure rotational and rovibrational lines of H_2 and possibly HD will provide a great thermometer for the bulk of the gas and pressure gradients inside the PDRs (e.g., Figure 4(a) and Parmar et al. 1991; Wright et al. 1999; Allers et al. 2005; Habart et al. 2005, 2011; Sheffer et al. 2011; Kaplan et al. 2017; Joblin et al. 2018).

These constraints on the physical conditions will be essential to study the dynamical effects in PDRs, e.g., compression waves, photoevaporative flows, ionization front, and dissociation front instabilities. Very precise determination of the offset between the ionization front and the dissociation front will be obtained, as well as, how this offset is affected by the shapes of the evaporative flows (Carlsten & Hartigan 2018). Moreover, JWST will probe the thin surface layers that are sufficiently heated to photoevaporate from the PDR.

These observations will allow for a better understanding of the physical and dynamical processes at work, identify pertinent signatures and diagnostic tracers for the different key PDR zones, improve model predictions for both warm molecular and ionized gas and help the development of new PDR models which couple the dynamics of photoevaporation to physico-chemical processes (e.g., Bron et al. 2018).

The role of dust properties (e.g., size distribution) in determining the position of the $H^+/H^0/H_2$ transition will also be better constrained with these observations (Allers et al. 2005; Schirmer et al. 2021). Moreover, grain surface chemistry is an unavoidable route for efficient H_2 formation (e.g., Gould & Salpeter 1963; Wakelam et al. 2017). Observations of numerous H_2 rotational and rovibrational lines at high spatial resolution might constrain both the H_2 formation processes in warm gas and grains and the mechanisms that control the H_2 ortho-para ratio (e.g., Habart et al. 2004; Bron et al. 2014, 2016). Determination of the H_2 formation rate on interstellar grains and its abundance is particularly important, as it controls most of the PDR physical structure and subsequent development of the chemical complexity in the ISM (for a review on H_2 formation in the ISM see Wakelam et al. 2017).

Possibly, highly excited rotational and rovibrational lines of CO, H_2O, HDO, OH, CH^+ will also lead to a better understanding of the radiative and chemical pumping in PDRs. These lines will also be particularly useful to constrain the physical properties of the high-pressure components present in PDRs. Complemented by velocity resolved observations at high angular resolution obtained with radio interferometers, they will provide key insights into the dynamical activity

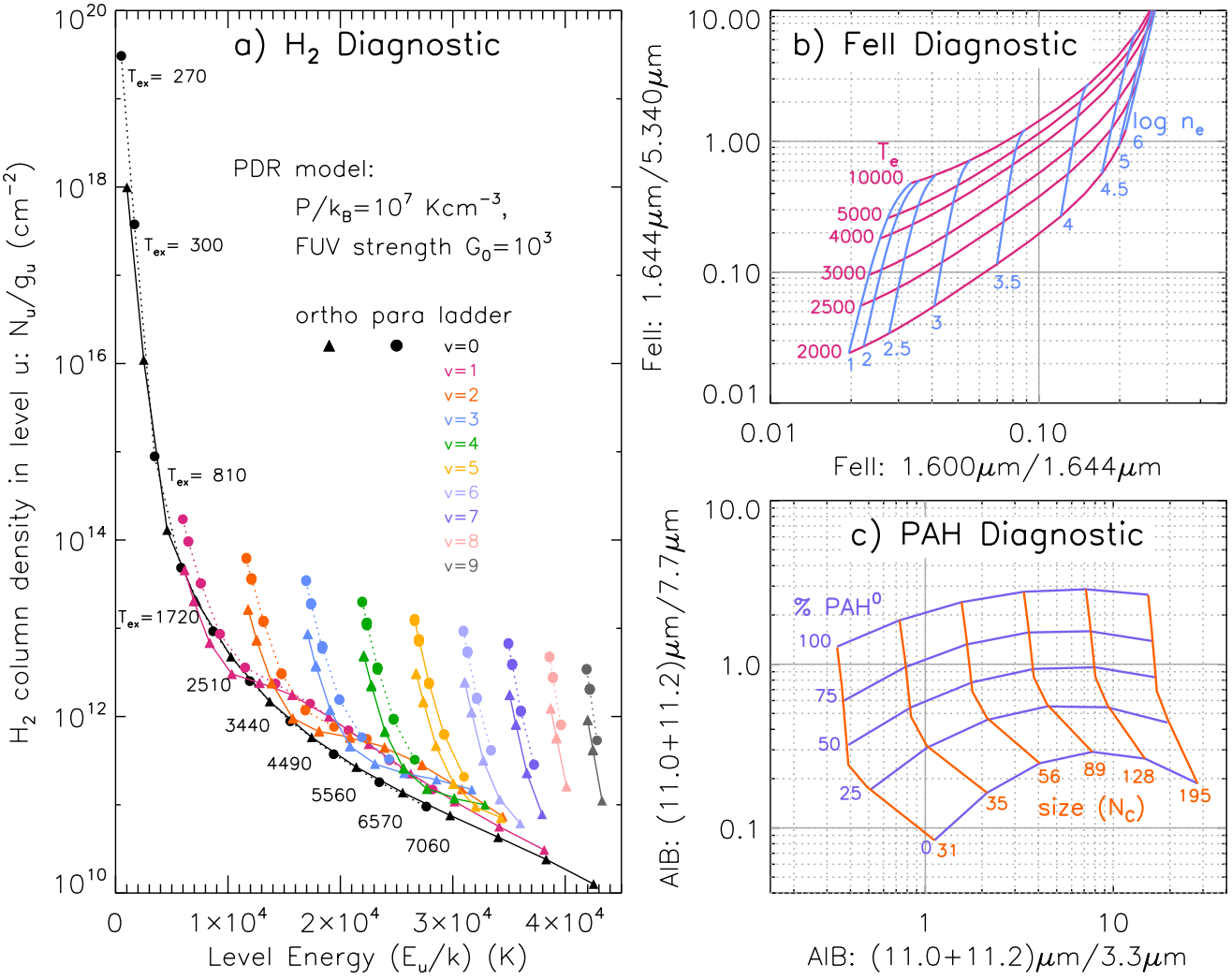

Figure 4. Example IR PDR diagnostics: (a) Excitation diagram from H_2 lines in PDRs, that are observable by MIRI and NIRSpec, as a tracer of the warm and hot (UV-pumped) excitation temperatures (excitation temperatures derived from the level populations by a local Boltzmann fit are indicated); (b) The [Fe II] lines as a tracer of the temperature and density distribution from the ionized gas to the PDR (Del Zanna et al. 2021 and using atomic data from Deb & Hibbert 2011 and Smyth et al. 2019); (c) AIB emission ratios as a tracer of PAH size (in function of the number of carbon atoms, N_C) and charge (in function of the neutral PAHs fraction, i.e., $PAH^0/(PAH^0+PAH^1)$), computed from harmonic IR spectra using PAHdb and assuming an interstellar radiation field (see Section 8 for a description of PAHdb). Figure adapted from Maragkoudakis et al. (2020).

(turbulence, photoevaporation) of the PDR. The presence of large columns of vibrationally excited H_2 that help to overcome certain reactions drive the endothermic carbon chemistry (e.g., Sternberg & Dalgarno 1995; Agúndez et al. 2010). Mid-IR superthermal emission of OH will probe the far-UV dissociation of H_2O and measure the local irradiation and density conditions (Tabone et al. 2021). Finally, rovibrational lines of non-polar molecules (e.g., CH_4, C_2H_2, C_6H_6) will give a more complete inventory of hydrocarbon species and better characterize their formation/destruction processes via top-down or bottom-up chemistry (e.g., Cernicharo 2004; Parker et al. 2012; Contreras & Salama 2013; Pilleri et al. 2013; Alata et al. 2014; Guzmán et al. 2015; Jones & Habart 2015; Sciamma-O'Brien & Salama 2020).

Photochemical evolution of carbonaceous species—A key spectroscopic feature of PDRs is the AIBs, observed throughout the universe at 3.3, 6.2, 7.7, 8.6, and 11.2 μm (see Figure 2) and attributed to the infrared fluorescence of nanometric particles and molecules from the family of Polycyclic Aromatic Hydrocarbons (PAHs) (Leger & Puget 1984; Allamandola et al. 1985). In addition to interstellar PAHs, emission from the fullerene C_{60} is also present in PDRs, characterized by emission bands detected at 7.0, 17.4, and 18.9 μm (Sellgren et al. 2010; Boersma et al. 2012; Peeters et al.

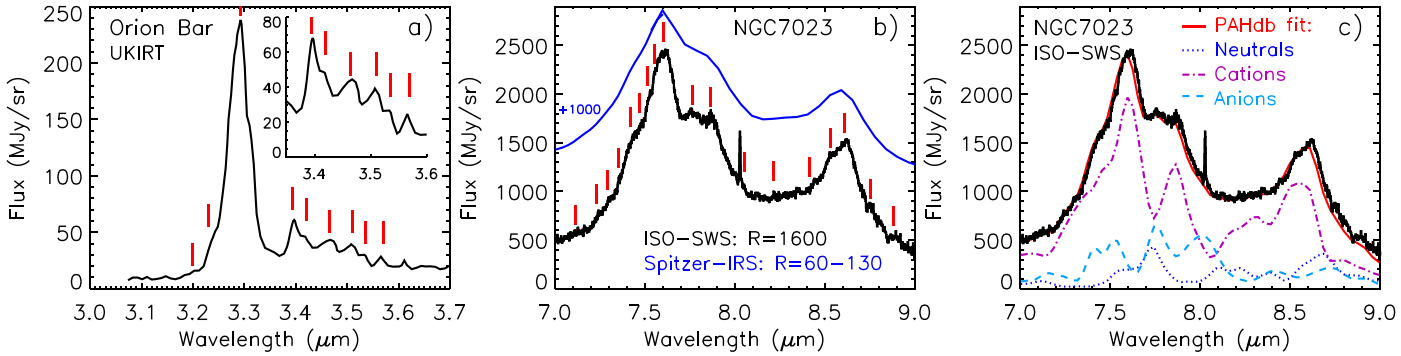

Figure 5. The spectral richness of the AIB emission toward two prototypical PDRs shown for (a) the 3 μm and (b) the 8 μm region (Geballe et al. 1989; Moutou et al. 1999). The inset in panel a zooms in on the 3.4–3.6 μm region. Vertical bars indicate sub-structure (reflecting sub-components). These are not detectable at low spectral resolution (panel b, blue line, offset = 1000). (c) PAHdb fitting to the 7–9 μm range shown with its breakdown in charge states (see Section 8 for a description of PAHdb).

2012; Castellanos et al. 2014; Berné et al. 2017). The underlying continuum present in mid-IR spectra (Figure 2) is more difficult to attribute, but is believed to be due to some form of very small carbonaceous grains (VSGs, Désert et al. 1990; Compiègne et al. 2011), amorphous hydrocarbon nanoparticles (Jones et al. 2013) and/or PAH clusters (Rapacioli et al. 2006). In regions closest to massive stars, large silicate grains can also emit in the mid-IR continuum (Cesarsky et al. 2000; Knight et al. 2022).

An important aspect of these spectroscopic features is that their relative contributions to the mid-IR spectrum vary significantly (e.g., Cesarsky et al. 1996; Joblin et al. 1996a; Sloan et al. 1997; Peeters et al. 2002; Rapacioli et al. 2005; Compiègne et al. 2007; Povich et al. 2007; Watson et al. 2008; Boersma et al. 2012; Candian et al. 2012; Mori et al. 2012, 2014; Stock et al. 2016; Sidhu et al. 2021). These variations suggest an evolution from VSGs with a possible mixed aromatic aliphatic nature present in UV shielded regions, to free-flying PAH species at the surface of molecular clouds (Rapacioli et al. 2005; Berné et al. 2012; Pilleri et al. 2015; Peeters et al. 2017; Murga et al. 2020; Schirmer et al. 2020), and eventually to more stable fullerenes (Berné et al. 2015) and GrandPAHs (i.e., the most stable PAHs; Andrews et al. 2015) in harsh (high G_0) environments. This evolution in PDRs has strong implications for the understanding of the PDR physics, notably the local extinction of the UV field, the heating of the gas (by the photoelectric effect), and the formation of H_2. Without detailed knowledge of the properties of these species, the implementation of these mechanisms in theoretical models can only be approximate. In addition, this general scenario needs however to be extended, by identifying the connection between the photochemical evolution of large carbonaceous species such as PAHs and fullerenes with other chemical networks of PDRs. One critical aspect concerns the link with small hydrocarbons such as acetylene or benzene. These non-polar species cannot be detected with radio-telescope, but their infrared band may be detected with JWST. Mapping the emission from these species in the Orion Bar at high angular resolution will offer unprecedented access to the organic inventory of a PDR, allowing to link chemical networks.

The combination of $R \sim 3000$ spectral resolution mid-IR spectroscopy of AIBs (resolving the plethora of AIB subcomponents and structure; see Figure 5) with detailed knowledge of the physical conditions will provide key constraints on astrochemical models of PAH evolution (e.g., Galliano et al. 2008; Montillaud et al. 2013; Mori et al. 2014; Andrews et al. 2015; Berné et al. 2015; Boersma et al. 2015; Croiset et al. 2016; Stock & Peeters 2017; Murga et al. 2019, 2022; Dartois et al. 2020; Knight et al. 2021, 2022), which will help determine the dominant properties of PAH populations. This will in turn guide laboratory experiments or quantum chemical calculations which provide the molecular parameters these models rely on (e.g., Maltseva et al. 2015; Sabbah et al. 2017; Salama et al. 2018; Dartois et al. 2020; Martínez et al. 2020; Wiersma et al. 2020; Gatchell et al. 2021; Zettergren et al. 2021). Overall, this synergy between observations, models, laboratory experiments and theory is essential to determining the properties and role of PAHs and related carbonaceous species in space (see Joblin & Tielens 2011 and references therein).

Finally, the comparison of JWST observations with dust emission models will also be essential to constrain the dust evolution on a small scale at the edge of the PDR. Earlier studies using suggest that the abundance of VSGs is reduced in a variety of PDRs (e.g., in filaments of the Taurus cloud, the Horsehead, and NGC 2023/7023 nebula, Stepnik et al. 2003; Compiègne et al. 2008; Arab et al. 2012), but it is unclear what the origin of this depletion is.

Interpretation of unresolved PDRs—The JWST spectra of various types of objects (typically galaxies or UV-irradiated protoplanetary disks) will be dominated by PDR emission which is spatially unresolved. Deriving the physical conditions

in these sources, where the emission from all PDR components is blended in one or a few spectra, is therefore much more difficult. This ERS program will provide Science-Enabling Products that will facilitate the interpretation of unresolved PDRs (Section 8). For instance, we will provide a collection of template spectra extracted from the observations, with two different methods (see Section 8), which can be used to help interpret spectra of unresolved sources. We will extend existing data-analysis tools and line and AIB diagnostic tools into the JWST era and validate them on the ERS data from this program. This approach has been highly successful in the past: tools which were benchmarked on galactic star-forming regions or nearby galaxies, such as PDR models (e.g., the Meudon code Le Petit et al. 2006, the Kosma-Tau PDR code Röllig et al. 2013, the Kaufman et al. 1999 model, the UCL-PDR model Bell et al. 2006) or spectroscopic decomposition tools (e.g., PAHFIT Smith et al. 2007, PAHTAT Pilleri et al. 2012) have also been widely used for the analysis and the determination of physical conditions in external galaxies (e.g., Malhotra et al. 2001; Bayet et al. 2009; Cormier et al. 2012; Naslim et al. 2015; Chevance et al. 2016) or disks (Berné et al. 2009; Champion et al. 2017; Vicente et al. 2013).

6. Simulated Spectra

In order to illustrate the spectral richness that JWST will observe and to perform signal-to-noise ratio (S/N) calculations, we modeled the IR emission of the 4 key regions between the interface of the H II region around the massive stars and the molecular gas (Figure 1), for the case of the Orion Bar (Section 4). These spectra are also used by our team to create simulations of the future JWST observations to test the Science-Enabling Products (Section 8) and advanced data-processing algorithms (e.g., Guilloteau et al. 2020a, 2020b). Figure 6 shows the obtained model templates at a spectral resolving power of 3000 illustrating the contribution of ionic, atomic, and molecular gas lines, AIBs, small dust bands, dust scattered light, and continuum emission. The spectra are available in numerical format from [link to be inserted upon publication]. The four spectra have been computed individually for each region and each component using (i) the Cloudy code for the ionized gas in the H II region and the ionization front (Ferland et al. 2017); (ii) the Meudon PDR code for the contribution from the atomic and molecular lines in the neutral PDR gas (Le Petit et al. 2006); (iii) the AIB spectra extracted by Foschino et al. (2019); and (iv) the DustEM tool and SOC radiative transfer code for the contribution from the dust continuum and scattered light (Compiègne et al. 2011; Juvela 2019; Schirmer et al. 2021). Below we briefly describe the parameters and calculation requirements used for each model and region. The physical parameters used for these models correspond to those of the Orion Bar described in Section 4.

Ionized gas emission. For the ionized gas component we rely on the Cloudy code (Ferland et al. 2017). We adopt the same model parameters as in Shaw et al. (2009) and Pellegrini et al. (2009). An illuminating star characterized by a Kurucz star model with an effective temperature $T_{\rm eff} = 39{,}600$ K was considered. The total number of ionizing photons emitted by the star is set to $Q_{\rm LyC} = 9.8 \times 10^{48}$ photon s^{-1}. For the density, the initial electronic density is assumed to be $n_e^0 = 3160$ cm^{-3}, and a constant pressure was assumed.

Molecular and neutral atomic gas emission. For this component, we rely on the Meudon PDR code. We consider an isobaric model with a thermal pressure $P = 4 \times 10^8$ K cm^{-3} based on Joblin et al. (2018). We fix the radiation field impinging on the PDR so that, at the edge of the PDR, $G_0 = 2.25 \times 10^4$ in Habing units (in agreement with previous estimates given $G_0 = (1\text{–}4) \times 10^4$ Tielens & Hollenbach 1985a; Marconi et al. 1998). We adopted the extinction curve of HD 38087 of Fitzpatrick & Massa (1990) and $R_V = 5.62$ which is close to the value determined for Orion Bar of 5.5 (Marconi et al. 1998). A complete transfer with an exact calculation of the mutual screening between the UV pumping lines of H_2 was done since it can have a significant effect on the position of the H/H_2 transition and it can impact the intensities of the rovibrational lines of the radiative cascade. To obtain the model template spectra, we calculate the cumulative line intensities from the atomic and H/H_2 transition region ($0 < A_V < 2.5$) and from the molecular region (which starts at the C/CO transition, $2.5 < A_V < 8.5$). We set an upper limit of $A_V = 8.5$ to the molecular region to eliminate emission caused by the interstellar radiation field on the back side. This PDR model provides a good agreement with the observed values of the high-J CO emission produced before the C^+/C/CO transition and that originate from small structures of a typical thickness of a few 10^{-3} pc or $\sim 1''$ (Joblin et al. 2018). To reproduce the nearly edge-on geometry of the Bar (Hogerheijde et al. 1995; Jansen et al. 1995; Wen & O'dell 1995; Walmsley et al. 2000), we adopt a geometry in which the PDR is observed with a viewing angle θ between the line-of-sight and the normal to the PDR equal to $\sim 60°$. This angle is defined with 0° being face-on and 90° edge-on. The value of 60° gives an approximation of a nearly edge-on PDR and is the maximum inclination that can be used to derive line intensities in the 1D PDR Meudon code. The optically thin line surface brightnesses are enhanced by a geometrical factor of $1/\cos(\theta) = 2$ relative to their face-on surface brightnesses. The uncertainty on this angle could lead to an additional scaling factor on all line intensities.

Dust emission and scattering. To compute the dust emission and scattering in the neutral zone, we use the THEMIS[108] interstellar dust model together with the 3D radiative transfer code

[108] The Heterogeneous dust Evolution Model for Interstellar Solids, available here: https://www.ias.u-psud.fr/themis/. See model overview in Jones et al. (2017) and references therein.

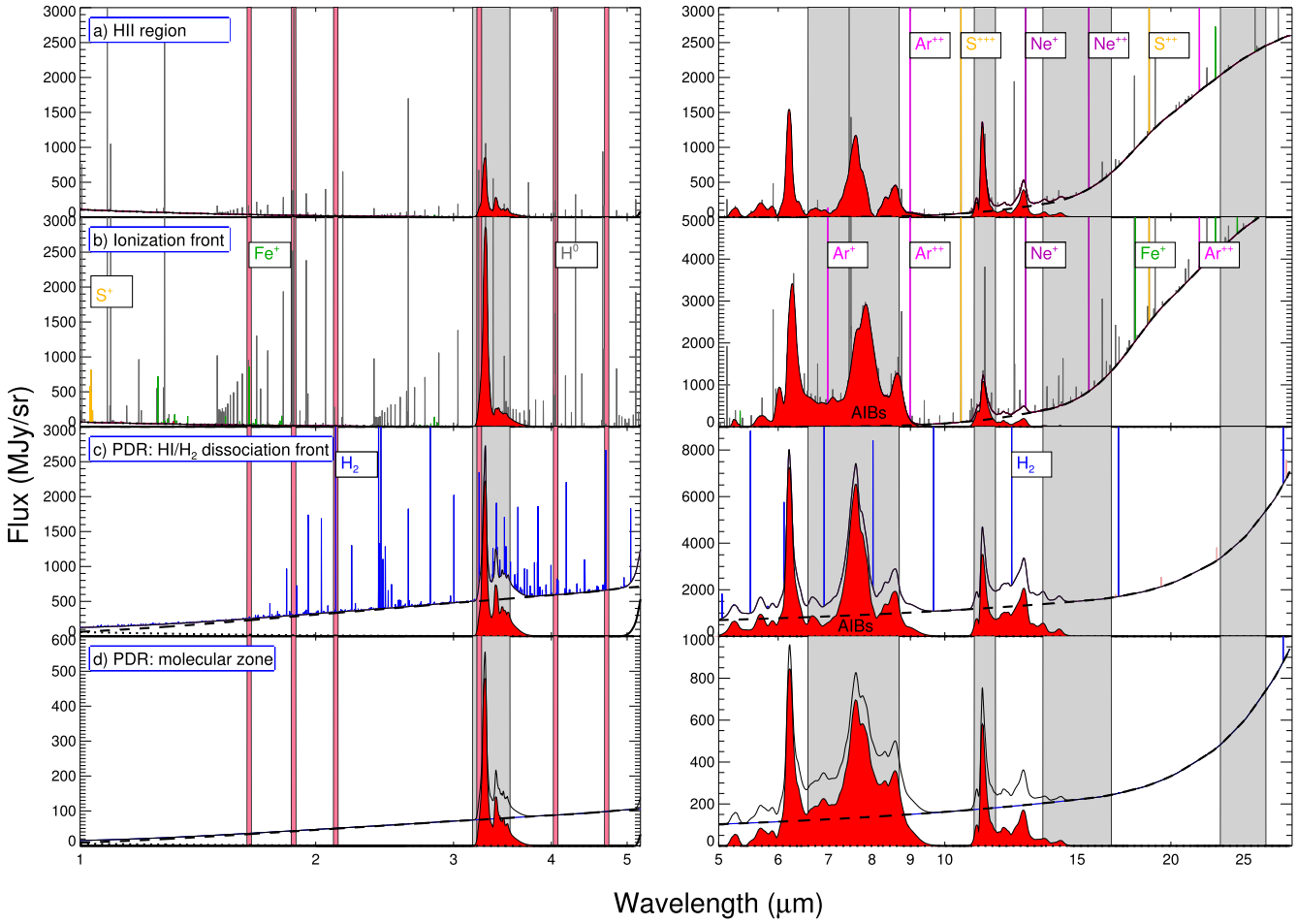

Figure 6. Model IR spectra at a spectral resolving power of 3000 of the 4 key regions within the interface of the H II region around the massive stars and the molecular gas (Figure 1) illustrating the spectral richness that JWST will observe. Dust-scattered light and continuum emission are shown in dotted and dashed lines. Ionic, atomic, and molecular gas lines are shown in colors (gray, green, pink, purple, blue). Aromatic and small dust bands are shown in red. The bandpass of the photometric filters selected in this ERS program is shown in gray and pink for the medium and narrow filters respectively. Spectra have been calculated with the Cloudy (Ferland et al. 2017), Meudon PDR code (Le Petit et al. 2006), the spectra from Foschino et al. (2019) for the PAH emission, and the DustEM (Compiègne et al. 2011) and THEMIS/SOC models (Schirmer et al. 2022) for the dust emission and scattering.

SOC following the approach of Schirmer et al. (2020). We consider the density profile toward the Orion Bar described in Arab et al. (2012) which agrees with the dust observational constraints from Spitzer and Herschel. A radiation field corresponding to a star of $T_{\rm eff} = 40{,}000$ K with $G_0 = 2{,}25 \times 10^4$ in Habing units is used. The dust size distributions were adjusted in order to reproduce the IR observations of the Orion Bar (Spitzer IRAC 3.6, 4.5, 5.8, and 8 μm, Herschel PACS, 70 and 160 μm, and SPIRE 250, 350, and 500 μm): the amorphous hydrocarbon nano-particle to gas ratio is set to about 100 times lower and their minimum size is set to 1.8 times larger than in the diffuse ISM (Schirmer et al. 2022). For the model template spectra of the atomic and H/H_2 transition region (Figure 6(c)), we calculate the average of the emission from the edge of the PDR up to a column density, from the edge, of 4.6×10^{21} H cm^{-2}, corresponding to the depth of the C/CO transition as computed by the PDR Meudon code (see above). For the molecular region (Figure 6(d)), we calculate the average of the emission from the layers which begins after the C/CO transition and ends at a density column from the edge of the PDR of 1.6×10^{22} H cm^{-2}. For the calculation of the dust continuum and scattered light in the ionized region and ionization front, we used the DustEM optically thin model (Compiègne et al. 2011). The incident spectrum on the H II region and the transmitted spectrum in the ionization front calculated by Cloudy was used.

Aromatic infrared band emission. For each region, we also define a normalized (over the area) spectrum for AIB emission. These are computed using the four template spectra extracted by Foschino et al. (2019) on ISO SWS data using machine learning algorithms. The four spectra represent four families of

Table 1
Filter Selection for NIRCam and MIRI

Species	λ[a] (μm)	Filter	Cont. Filter[b]	OB[c]	NGC 1982[c]
		NIRCam			
[Fe II]	1.644	F164N	F162M	√	
Paα	1.876	F187N	F182M	√	√
Brα	4.052	F405N	F410M	√	√
H_2	2.120	F212N	F210M	√	√
H_2	3.235	F323N[4]	F300M	√	
H_2	4.694	F470N	F480M	√	
AIB	3.3	F335M	F300M	√	√
	1.405	F140M		√	
	1.659	F150W2		√	
	2.672	F277W		√	
	3.232	F322W2		√	
	4.408	F444W		√	√
		MIRI			
	7.7	F770W		√	
	11.3	F1130W		√	
	15.0	F1500W		√	
	25.5	F2550W		√	

Notes.
[a] The wavelength of the transition or the pivot wavelength of the filter for NIRCam broad band filters.
[b] Continuum filter;
[c] OB: Orion Bar (on-target observations); NGC 1982: NIRCam parallel observations;
[d] This filter is not contaminated by the 3.3 μm AIB.

PAH-related species, namely neutral PAHs (PAH^0), cationic PAHs (PAH^+), evaporating very small grains (eVSGs), and large ionized PAHs (PAH^x). The description of these species is given in Pilleri et al. (2012, 2015) and Foschino et al. (2019). For the H II region, the PAH spectrum consists completely of PAH^0, since the abundance of electrons is large and hence recombination of cationic PAHs is very efficient at keeping molecules neutral. At the ionization front, PAH emission is dominated by the neutral side of the interface, where density is highest, where gas is mostly neutral, and where the radiation field is high. Therefore, recombination with electrons is highly ineffective and only cationic PAHs, in particular the largest, can survive. This type of environment is similar to that of planetary nebulae where PAH^x are dominant (Joblin et al. 2008), hence we use this spectrum for the ionization front. On the dissociation front, emission is dominated by neutral PAHs but with a contribution of cations (see e.g., Berné et al. 2012), hence we adopt a spectrum consisting of 60% PAH^0 and 40% PAH^+. Finally, the molecular cloud region is dominated by eVSG and neutral PAHs, as seen in e.g., NGC 7023 (Berné et al. 2012), and we adopt a spectrum with half eVSG and half PAH^0. The normalized AIB spectra were scaled to reproduce the integrated fluxes as observed in the Orion bar by Spitzer.

Absolute calibration and recommended use of the spectra. Absolute calibration of the total spectrum resulting from the sum of the four different regions has been cross-checked with existing observations of the Orion Bar (ISO, Spitzer, SOFI/NTT, HST), so as to confirm that the total spectrum is roughly realistic in terms of flux units. Moreover, for some specific gas lines (e.g., [Fe II], H_2) observed recently with the Keck telescope at very high angular resolution ($\sim 0\farcs1$), we compare our model predictions to the observed peak emission at the ionization front and dissociation front (E. Habart et al. 2022, in preparation). This allowed us to ensure that we do not underestimate the peak emission by important factors. We emphasize that the individual spectra of the different regions, obtained by making simple assumptions and by separately estimating the different components (ionized gas, neutral gas, dust in ionized gas, dust in neutral gas, PAHs) are not fully realistic. However, these spectra can be useful for time estimates with the JWST time exposure calculator, or testing data-analysis tools, before obtaining actual data.

7. Observations

The program objectives (Sections 3, 5) require the use of near- and mid-IR spatially resolved spectroscopy to extract the spectra and signatures of the critical sub-regions in a PDR (Figures 1, 3), and near- and mid-IR imaging to obtain a general understanding of the environment. Hereafter we describe in detail the set of planned observations as part of this ERS project with MIRI, NIRSpec, and NIRCam. For the imaging, the filter selection is given in Table 1. The file containing the details of these observations can be downloaded directly in the Astronomer Proposal Toolkit (APT) using the program ID 1288.

7.1. NIRSpec IFU Spectroscopy

We will obtain a 9×1 mosaic centered on position $\alpha = 05\ 35\ 20.4864$, $\delta = -05\ 25\ 10.96$ (Figure 3) for the 1–5.3 μm range. The exact position angle (PA) for the mosaic will depend on the date of observation, however, we plan to have PA $\sim 60°$. We use the H grisms with a spectral resolution of $\sim$2700, the NRSRAPID readout mode, which is appropriate for bright sources, and a 4-point dither. We include a dark exposure to quantify the leakage of the Micro-Shutter Array (MSA).[109] We use five groups per integration with one integration and one exposure for a total on-source integration time of 257.7 s.[110] The expected S/Ns have been computed using the Exposure Time Calculator (ETC)[111] provided by

[109] https://jwst-docs.stsci.edu/jwst-near-infrared-spectrograph/nirspec-operations/nirspec-ifu-operations/nirspec-msa-leakage-correction-for-ifu-observations
[110] Definitions of groups, integrations, and exposures can be found at https://jwst-docs.stsci.edu/understanding-exposure-times.
[111] https://jwst.etc.stsci.edu/

STScI, based on a reference spectrum which is the average of the four template spectra described in Section 6. This provides an S/N per spectral resolution element on the continuum of at least 25, and up to several hundred for the 3.3 μm PAH band, and up to a few thousand on bright lines. In Canin et al. (2022) we provide a detailed simulation of the NIRSpec-IFU observations of the Orion Bar.

7.2. MIRI IFU Spectroscopy

We will obtain a 7×2 mosaic centered on position $\alpha = 05$ 35 20.4869, $\delta = -05$ 25 11.02 (Figure 3) over the entire 5–28.5 μm range, also with a PA $\sim 60°$. We note that the NIRspec IFU spectroscopy mosaic described above is fully included in the MIRI IFU mosaic, the latter being larger, especially at longer wavelengths due to instrument design (Rieke et al. 2015). We use the MRS spectrometer with a spectral resolution of $\sim$3000. We apply a 4-point dither optimized for extended sources and use the FASTR1 readout mode and the SUB128 imager subarray, both adapted for bright sources. We integrate 111s using 10 groups per integration with one integration and one exposure. According to the ETC, using our reference spectrum yields a minimal S/N per spectral resolution element of $\sim$10 on the continuum, and up to above 500 for bright lines and PAH bands.

7.3. NIRCam Imaging

We will observe (i) the 3.3 μm PAH band which, when combined with the 11.3 μm PAH band, measures PAH size (Figure 4(c); Ricca et al. 2012; Croiset et al. 2016; Knight et al. 2021), (ii) the vibrationally excited lines of H_2 at 2.12, 3.23, and 4.7 μm, tracing the dissociation front, (iii) the [Fe II] at 1.64 μm, tracing the ionization front, and (iv) the Paα and Brα lines, tracing the H II region. For each, we include a reference filter for the subtraction of the underlying continuum emission. We will also obtain broad band observations at 1.5, 2.7, 3.2, and 4.4 μm. We will map the PDR region with a single pointing using a 4-point dither (Figure 7). All used filters are summarized in Table 1. We use the RAPID readout mode since the Orion Bar is very bright. We will obtain an S/N on the extended emission above 10 for all filters with a total on-source exposure time of 85.9 s (2 groups per integration, one integration, and one exposure).

7.4. MIRI Imaging

We will observe (i) the 7.7 μm PAH band, (ii) the 11.3 μm PAH band which, when combined, provide a proxy for PAH ionization (e.g., Joblin et al. 1996b; Hony et al. 2001), (iii) VSGs (Désert et al. 1990), and (iv) continuum emission at 25 μm, tracing warm dust in the H II region, similarly to the corresponding WISE, Spitzer, and IRAS filters. We obtain a 3×3 mosaic using 2 dithers and a 2-point dither pattern (2-POINT-MIRI-F770W-WITH-NIRCam) with 4 pointings (Figure 7). To accommodate the brightness of the Orion Bar, we use the FASTR1 reading mode and the SUB128 imager subarray. We obtain an S/N above 10 with a total on-source integration time of 136.9 s (5 groups per integration, 115 integrations, and 1 exposure).

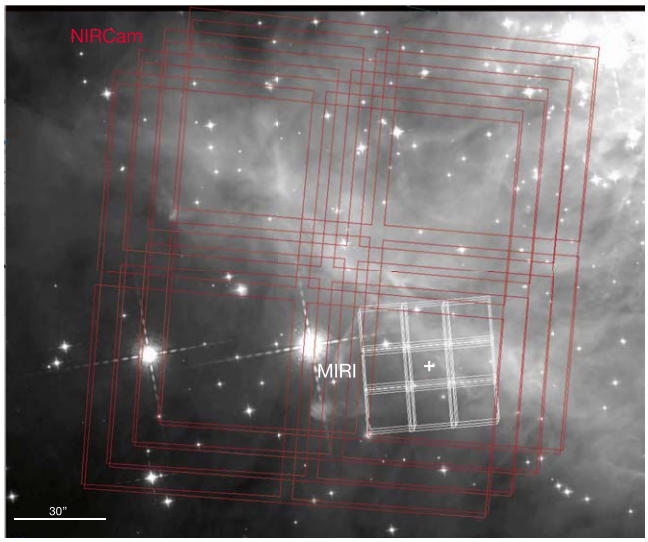

Figure 7. Overlay of the JWST NIRCam (red) and MIRI (white) imaging footprints on the Hubble Space Telescope image of the Orion Bar at 1.3 μm (Robberto et al. 2020). MIRI observations are centered on position $\alpha = 05$ 35 20.3448 and $\delta = -05$ 25 4.01 (position indicated by the white cross). For NIRCam, only module B covering the Bar is shown in this overlay. Module A is situated to the North (outside of the image), and the pointing position (also outside this image) is situated in between these two modules at $\alpha = 05$ 35 20.1963, $\delta = -05$ 23 10.45.

7.5. NIRCam Parallel Observations

We will obtain parallel NIRCam observations with the on-source MIRI imaging. The exact FOV will depend on the time of observations. If the observations are taken in the September visibility window (as we expect as of today), it will be located North of the Orion Bar, in the NGC 1982 region. We will observe (i) the 3.3 μm PAH band, (ii) the vibrationally excited line of H_2 at 2.12 μm, and (iii) the Paα and Brα lines. For each, we include a reference filter for the subtraction of the underlying continuum emission. We will also obtain a broad band observation at 4.4 μm. The filters for these observations are summarized in Table 1. The pointings, number of dithers, and dither pattern are set by those of the primary observations (on-source MIRI imaging). To accommodate the brightness of the Orion Bar, we will use the BRIGHT2 readout mode and will obtain a total integration time of 128.8 s (using 2 groups per integration, 1 integration, and 1 exposure).

7.6. "Off" Observations

We include spectroscopic "off" observations to subtract any undesirable emission from scattered light from the Sun or the Galactic plane, telescope emission, Zodiacal light, or instrumental signal. This ensures the highest quality data, and provides information on possible background sources. We have chosen a background position (same for both instruments) situated in a region of very low emission in 2MASS and WISE surveys at a distance of 2° from our on-source observations at $\alpha = 05\ 27\ 19.40$ and $\delta = -05\ 32\ 4.40$.

7.7. Risks of Saturation: Estimates and Mitigation

We have conducted a number of tests to estimate and mitigate the risks of saturation.

For the spectroscopic observations, the standard ETC calculations do not show any warning of saturation when employing a reference spectrum of the Orion Bar. However, the true (peak) intensities could be underestimated due to the increased spatial and spectral resolution of JWST compared to prior observations. We, therefore, took a conservative approach and investigated potential risks when employing this reference spectrum multiplied by a factor of 3. For MIRI, we obtain partial saturation[112] in the [Ne II] line at 12.8 μm and in the [S III] line at 18.7 μm. This risk is thus mainly affecting the part of the mosaic situated in the H II region and only concerns these lines (i.e., the rest of the spectrum is not saturated in this exercise). Since the saturation is only partial and the integration ramps are usable up to when the saturation occurs, we expect that fluxes can still be recovered for these lines. We do not see any saturation issues with NIRSpec. Regarding the photometric observations, we apply the same method to probe potential risks. For NIRCam observations, the ETC calculations do not show any warnings using the reference spectrum nor this spectrum multiplied by a factor of 3 (assuming an extended source). Discussions with instrument teams suggest that saturation with NIRCam on the Orion Bar in the extended emission is highly unlikely. We have also run detailed modeling of the observations using the MIRAGE instrument simulator,[113] inserting background images of the Orion Bar at appropriate wavelengths from Hubble or Spitzer (Canin et al. 2021). These simulated data do not show any saturation in the extended emission. For saturation of point sources, we ran the MIRAGE simulator inserting a point source with the magnitude of θ^2 Ori A (Canin et al. 2021). The star saturates the detector but only in a few pixels at the position of the star. Stray light is also limited to the immediate surroundings of the star. Overall, our predictions suggest that the risk of saturation for NIRCam on the Orion Bar is low. For MIRI imaging, the ETC predicts that the Orion Bar saturates the detectors in all filters if the full array is used for an extended source with the reference spectrum multiplied by 3. We have therefore modified the observations and adopted a strategy which consists in reading the detector much faster only on a sub-field of 128 × 128 pixels (SUB128) to avoid saturation. The resulting field of view is thus much smaller, hence to cover a large enough region, we must perform a 3 × 3 mosaic (Figure 7). This is more time consuming than a standard strategy, however, this is the only approach to limit the risks of saturation.

[112] Partial saturation indicates saturation occurs in the third group or a later group of the integration ramp (https://jwst-docs.stsci.edu/jwst-exposure-time-calculator-overview/jwst-etc-calculations-page-overview/jwst-etc-saturation).

[113] https://github.com/spacetelescope/mirage

8. Science-enabling Products (SEPs)

In the context of this ERS project, we will provide three types of SEPs to the community: (1) enhanced data products, (2) products facilitating data reduction and processing, and (3) data-interpretation tools via STScI and our website.[114] First, we will provide the following enhanced data products:

1. Highly processed data products of the obtained observations. We will provide the data in a post-pipeline format (Stage 3). We will also provide highly processed data, in particular, stitched IFU cubes for NIRSpec and MIRI.
2. Maps of spectral features. Using the spectral decomposition tool PAHFIT (see below, Smith et al. 2007), we will produce integrated line and band maps, with uncertainties, from our IFU spectroscopy observations. The final products will be maps (FITS files) in physical units and astrometry.
3. Template spectra. We will obtain template PDR spectra from the observations using two separate methods. First, we will directly extract from the observations templates for each specific key zones (H II, IF, DF, MC). These 4 templates from the individual regions will primarily illustrate early in the mission the typical spectral signatures for classical regions in PDRs and will be useful to identify which conditions are present when observing an unresolved region. For instance, if a spatially unresolved JWST spectrum shows H_2 rotational lines and [Fe II] lines, an analogy with these template spectra can be used to assess that there is a mixture of warm molecular gas and hot ionized gas. Second, we will use blind signal separation methods, following earlier work by Berné et al. (2007) and more recently Foschino et al. (2019), to extract underlying emission of AIB populations. Following Pilleri et al. (2012) we will implement these templates in a new version of the PAHTAT fitting tool aimed at analyzing AIB emission.

Second, to facilitate post-pipeline data reduction and processing of similar JWST observations, we will deliver:

1. Spectral order stitching and stitched cubes. The official JWST pipeline assumes that combining spectra taken

[114] http://pdrs4all.org

with different gratings and/or settings can be done without any specific matching step. This is a success-oriented view, however past experience (with e.g., Spitzer-IRS, ISO-SWS) has shown that extra corrections are usually needed to provide smooth transitions between such spectral segments. We will quantify any spectral stitching issues. If needed, we will develop a Python-based tool to provide the needed extra corrections and, if possible, make it automated.

2. Cross-correlation of spectra and images. For the overlapping photometric and spectroscopic FOVs, a comparison will be done between the flux in specific (spectroscopic) lines or bands and the flux observed in specific (photometric) filters or combinations of filters (narrow and/or wide). This will be used for cross-calibration purposes and to define color correction for fields with bright PAH bands (e.g., Reach et al. 2005). The products will be correlation tables and simple mathematical recipes.
3. PAHFIT. This tool decomposes a spectrum into gas lines, dust features (aromatic/PAHs, aliphatics, fullerenes, silicates, ices), and dust continuum components and was developed for the analysis of Spitzer-IRS observations (Smith et al. 2007). Recently, Lai et al. (2020) applied it to AKARI-Spitzer observations. We will extend its capabilities to include JWST applicability, various decomposition methods for dust features and continuum, and various extinction determination methods (silicate absorption, H_2 lines) so it becomes more versatile. In addition, we will make sure it can automatically treat all pixels in IFU maps. This is implemented as a community open-source Python project (https://github.com/PAHFIT/pahfit).
4. Line list of all the lines and bands present in the data. The final product will be an ASCII table with the wavelength position, characteristic (line or band), and assignment of each line. For the lines, upper energy levels and Einstein coefficients for spontaneous emission will be added.

We will also provide an extensive and powerful set of tools for the interpretation of JWST data:

1. H_2 fitting tool will provide fits of observed H_2 excitation diagrams (e.g., Figure 4) for any pixel and yield the warm and hot (UV-pumped) excitation temperatures (T_{ex}), warm, hot, and total column densities (N_{H_2}), and ortho-to-para ratio (R_{otp}). Outputs will be excitation diagrams and maps of T_{ex}, N_{H_2} and R_{otp}. The tool will be part of the PDR Toolbox Pound & Wolfire (2008), http://dustem.astro.umd.edu, which has been rewritten as an open-source Python package (https://pdrtpy.readthedocs.io).
2. The interstellar medium database, ISMDB, is a model database with a web-based fitting tool to search in massive grids of state-of-the-art PDR models and derive physical parameters from observations of any number of spectral lines to be observed with JWST (http://ismdb.obspm.fr). This web service will give access to model grids from the Meudon PDR code (Le Petit et al. 2006) and the KOSMA-tau PDR code (Röllig et al. 2013). This tool will be able to handle maps of multiple lines (rather than single pointing observations in the existing version) and return the estimated parameter maps, providing in addition maps of the goodness-of-fit at each pixel and of the uncertainties at each pixel, as well single-pixel analysis tools allowing to visualize uncertainty correlations between the different parameters.
3. pyPAHdb Spectral Analysis Tool decomposes a PAH emission spectrum into contributing sub-populations (e.g., charge, size, composition, structure; Shannon & Boersma 2018). It is based on tools provided via the NASA Ames PAH IR Spectroscopic Database version 3.2 (PAHdb; http://www.astrochemistry.org/pahdb/, Cami 2011; Bauschlicher et al. 2010; Boersma et al. 2014; Bauschlicher et al. 2018; Mattioda et al. 2020), i.e., the AmesPAHdbIDLSuite and the AmesPAHdbPythonSuite (https://github.com/PAHdb/). The tool makes use of a matrix of pre-calculated emission spectra from version 3.20 of PAHdb's library of density-functional-theory computed absorption cross-sections. The products will be maps of the PAH ionization and large fraction. The tool is implemented as a community open-source Python project (https://github.com/PAHdb/pyPAHdb).
4. Ionized gas lines diagnostic diagrams. We will provide diagnostic diagrams of key species to be observed with JWST for the interpretation of ionized gas lines (Figure 4) and its conversion into physical conditions and extinction. These diagrams will be based on multi-level models or Cloudy (Ferland et al. 2017) and can be used for sources showing emission of ionized gas. This tool has recently been implemented in the PDR Toolbox (http://dustem.astro.umd.edu).

9. Community

The philosophy of this ERS program has been, from the start, to be open to the largest possible number of scientists, with the objective to gather together the international community. This has materialized into a large international, interdisciplinary, and diverse team of 145 scientists from 18 countries. The team includes observers, theoreticians, and experimentalists in the fields of astronomy, physics, and chemistry, and has a gender balance of 41% women (Figure 8). The program is led by the PI team (O. Berné, E. Habart & E. Peeters) who are assisted by a core team of 17 scientists.[115] This core team is complemented by

[115] The core team consists of A. Abergel, E. Bergin, J. Bernard-Salas, E. Bron, J. Cami, E. Dartois, A. Fuente, J. R. Goicoechea, K. Gordon, Y. Okada, T. Onaka, M. Robberto, M. Röllig, A. Tielens, S. Vicente, M. Wolfire.

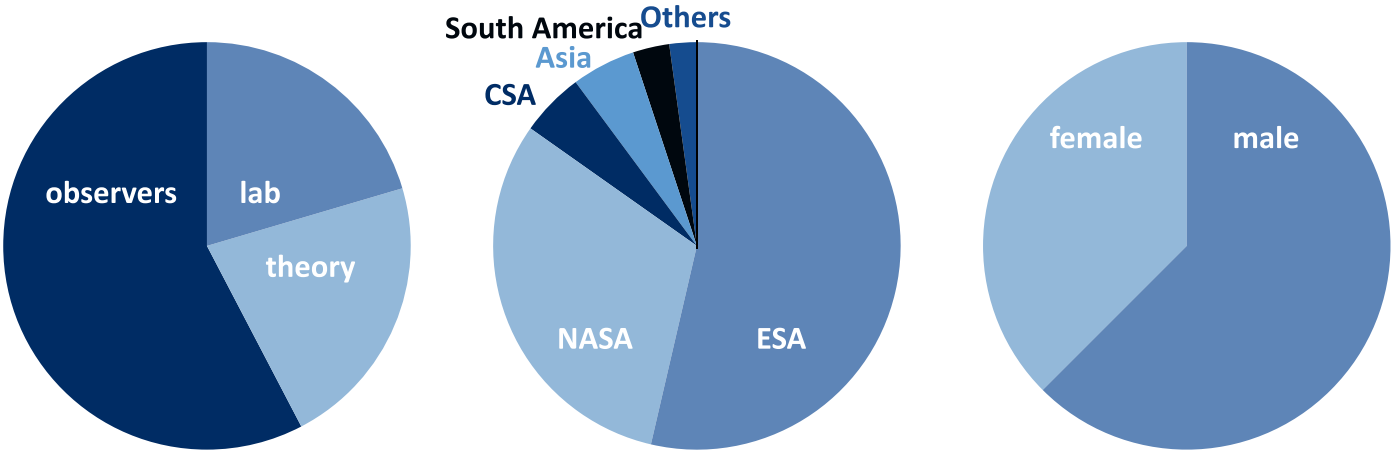

Figure 8. Detailed demographics of the PDRs4All team. The right chart represents the gender balance based on first names as given by the python package gender-guesser0.4.0. For the first names found in this database (90% of the team), results "female" and "mostly_female" were combined so were the results "male" and "mostly_male" while the result "androgynous" (1 name) was equally split over both genders.

extended-core team members who significantly contribute to the program, in particular with respect to the Science-Enabling Products. Telecons open to the community will be organized on a regular basis to disseminate data reduction and analysis techniques and recipes, best practices to design JWST proposals, and tutorials on the provided SEPs. We will organize the workshop "Galactic and extragalactic PDRs with JWST." For more information, please visit http://pdrs4all.org.

10. Conclusions

This paper presents the JWST ERS program PDRs4All: "Radiative feedback from massive stars." PDRs4All will be *the* go-to place for JWST observers who (1) are eager to see one of the first data taken with JWST, (2) are interested in how JWST's instruments perform on bright, extended targets, (3) need advanced software tools for the processing, analysis, and interpretation of JWST data, or (4) are simply interested in PDR physics and chemistry. Indeed, the unprecedented capabilities of JWST's instruments will give access to the key physical and chemical processes present in PDRs on the scale at which these processes occur. Therefore, without any exaggeration, PDRs4All will revolutionize our understanding of PDRs and provide major insight into the interpretation of unresolved PDRs, such as the surfaces of proto-planetary disks or distant star-forming galaxies.

We are grateful to the PAHFIT developers team (Karl Gordon, Thomas Lai, Alexandros Maragkoudakis, Els Peeters, Bethany Schefter, Ameek Sidhu, and J.D. Smith).

Support for JWST-ERS program ID 1288 was provided through grants from the STScI under NASA contract NAS5-03127 to STScI (K.G., D.V.D.P., M.R.), Univ. of Maryland (M.W., M.P.), Univ. of Michigan (E.B., F.A.), and Univ. of Toledo (T.S.-Y.L.).

O.B. and E.H. are supported by the Programme National "Physique et Chimie du Milieu Interstellaire" (PCMI) of CNRS/INSU with INC/INP co-funded by CEA and CNES, and through APR grants 6315 and 6410 provided by CNES. E. P. and J.C. acknowledge support from the National Science and Engineering Council of Canada (NSERC) Discovery Grant program (RGPIN-2020-06434 and RGPIN-2021-04197 respectively). E.P. acknowledges support from a Western Strategic Support Accelerator Grant (ROLA ID 0000050636). J.R.G. and S.C. thank the Spanish MCINN for funding support under grant PID2019-106110GB-I00. Work by M.R. and Y.O. is carried out within the Collaborative Research Centre 956, sub-project C1, funded by the Deutsche Forschungsgemeinschaft (DFG)—project ID 184018867. T.O. acknowledges support from JSPS Bilateral Program, grant No. 120219939. M.P. and M.W. acknowledge support from NASA Astrophysics Data Analysis Program award #80NSSC19K0573. C.B. is grateful for an appointment at NASA Ames Research Center through the San José State University Research Foundation (NNX17AJ88A) and acknowledges support from the Internal Scientist Funding Model (ISFM) Directed Work Package at NASA Ames titled: "Laboratory Astrophysics—The NASA Ames PAH IR Spectroscopic Database."

ORCID iDs

Olivier Berné https://orcid.org/0000-0002-1686-8395
Émilie Habart https://orcid.org/0000-0001-9136-8043
Els Peeters https://orcid.org/0000-0002-2541-1602
Alain Abergel https://orcid.org/0000-0003-2364-2260

Edwin A. Bergin https://orcid.org/0000-0003-4179-6394
Jeronimo Bernard-Salas https://orcid.org/0000-0002-8452-8675
Emeric Bron https://orcid.org/0000-0003-1532-7818
Jan Cami https://orcid.org/0000-0002-2666-9234
Emmanuel Dartois https://orcid.org/0000-0003-1197-7143
Asunción Fuente https://orcid.org/0000-0001-6317-6343
Javier R. Goicoechea https://orcid.org/0000-0001-7046-4319
Karl D. Gordon https://orcid.org/0000-0001-5340-6774
Yoko Okada https://orcid.org/0000-0002-6838-6435
Takashi Onaka https://orcid.org/0000-0002-8234-6747
Massimo Robberto https://orcid.org/0000-0002-9573-3199
Markus Röllig https://orcid.org/0000-0001-6205-2242
Alexander G. G. M. Tielens https://orcid.org/0000-0003-0306-0028
Sílvia Vicente https://orcid.org/0000-0001-8973-0752
Mark G. Wolfire https://orcid.org/0000-0003-0030-9510
Felipe Alarcón https://orcid.org/0000-0002-2692-7862
C. Boersma https://orcid.org/0000-0002-4836-217X
Amélie Canin https://orcid.org/0000-0002-7830-6363
Ryan Chown https://orcid.org/0000-0001-8241-7704
Daniel Dicken https://orcid.org/0000-0003-0589-5969
Romane Le Gal https://orcid.org/0000-0003-1837-3772
Marc W. Pound https://orcid.org/0000-0002-7269-342X
Boris Trahin https://orcid.org/0000-0001-5875-5340
Ameek Sidhu https://orcid.org/0000-0003-3771-4990
Dries Van De Putte https://orcid.org/0000-0002-5895-8268
Sara Cuadrado https://orcid.org/0000-0002-7393-1813
Claire Guilloteau https://orcid.org/0000-0001-5800-9647
Alexandros Maragkoudakis https://orcid.org/0000-0003-2552-3871
Bethany R. Schefter https://orcid.org/0000-0001-5080-8030
Thiébaut Schirmer https://orcid.org/0000-0002-8086-4890
Isabel Aleman https://orcid.org/0000-0002-7989-9041
Louis Allamandola https://orcid.org/0000-0002-6049-4079
Rebecca Auchettl https://orcid.org/0000-0001-9296-0751
Giuseppe Antonio Baratta https://orcid.org/0000-0002-3688-160X
Salma Bejaoui https://orcid.org/0000-0001-8646-9464
Partha P. Bera https://orcid.org/0000-0003-0843-3209
Goranka Bilalbegović https://orcid.org/0000-0002-1058-6610
John H. Black https://orcid.org/0000-0001-7221-7207
Francois Boulanger https://orcid.org/0000-0003-1097-6042
Jordy Bouwman https://orcid.org/0000-0002-3615-1703
Bernhard Brandl https://orcid.org/0000-0001-9737-169X
Sandra Brünken https://orcid.org/0000-0001-7175-4828
Andrew Burkhardt https://orcid.org/0000-0003-0799-0927
Alessandra Candian https://orcid.org/0000-0002-5431-4449
Jose Cernicharo https://orcid.org/0000-0002-3518-2524
Shubhadip Chakraborty https://orcid.org/0000-0002-2982-6450
Jason Champion https://orcid.org/0000-0002-9256-8917
Sean W. J. Colgan https://orcid.org/0000-0001-6275-7437
Ilsa R. Cooke https://orcid.org/0000-0002-0850-7426
Audrey Coutens https://orcid.org/0000-0003-1805-3920
Nick L. J. Cox https://orcid.org/0000-0002-7926-4492
Karine Demyk https://orcid.org/0000-0002-5019-8700
Jennifer Donovan Meyer https://orcid.org/0000-0002-3106-7676
Cécile Engrand https://orcid.org/0000-0002-0396-5583
Sacha Foschino https://orcid.org/0000-0003-2455-2355
Lisseth Gavilan https://orcid.org/0000-0001-8645-8415
Maryvonne Gerin https://orcid.org/0000-0002-2418-7952
Marie Godard https://orcid.org/0000-0002-7276-4021
Carl A. Gottlieb https://orcid.org/0000-0003-2845-5317
Pierre Guillard https://orcid.org/0000-0002-2421-1350
Antoine Gusdorf https://orcid.org/0000-0002-0354-1684
Patrick Hartigan https://orcid.org/0000-0002-5380-549X
Jinhua He https://orcid.org/0000-0002-3938-4393
Eric Herbst https://orcid.org/0000-0002-4649-2536
Liv Hornekaer https://orcid.org/0000-0003-0828-3642
Eduardo Janot-Pacheco https://orcid.org/0000-0003-0079-3912
Christine Joblin https://orcid.org/0000-0003-1561-6118
Michael Kaufman https://orcid.org/0000-0002-2521-1985
Francisca Kemper https://orcid.org/0000-0003-2743-8240
Sarah Kendrew https://orcid.org/0000-0002-7612-0469
Maria S. Kirsanova https://orcid.org/0000-0003-4338-9055
Pamela Klaassen https://orcid.org/0000-0001-9443-0463
Collin Knight https://orcid.org/0000-0003-2968-3522
Sun Kwok https://orcid.org/0000-0001-7708-081X
Álvaro Labiano https://orcid.org/0000-0002-0690-8824
Thomas S.-Y. Lai https://orcid.org/0000-0001-8490-6632
Timothy J. Lee https://orcid.org/0000-0002-2598-2237
Bertrand Lefloch https://orcid.org/0000-0002-9397-3826
Franck Le Petit https://orcid.org/0000-0001-8738-6724
Aigen Li https://orcid.org/0000-0002-1119-642X
Hendrik Linz https://orcid.org/0000-0002-8115-8437
Cameron J. Mackie https://orcid.org/0000-0003-2885-2021
Suzanne C. Madden https://orcid.org/0000-0003-3229-2899
Joëlle Mascetti https://orcid.org/0000-0002-8585-9118
Brett A. McGuire https://orcid.org/0000-0003-1254-4817
Pablo Merino https://orcid.org/0000-0002-0267-4020
Elisabetta R. Micelotta https://orcid.org/0000-0002-6555-5109
Jon A. Morse https://orcid.org/0000-0001-5895-2256
Giacomo Mulas https://orcid.org/0000-0003-0602-6669
Naslim Neelamkodan https://orcid.org/0000-0001-8901-7287
Ryou Ohsawa https://orcid.org/0000-0001-5797-6010
Alain Omont https://orcid.org/0000-0002-4721-3922

Roberta Paladini https://orcid.org/0000-0002-5158-243X
Maria Elisabetta Palumbo https://orcid.org/0000-0002-9122-491X
Amit Pathak https://orcid.org/0000-0001-6328-4512
Yvonne J. Pendleton https://orcid.org/0000-0001-8102-2903
Annemieke Petrignani https://orcid.org/0000-0002-6116-5867
Thomas Pino https://orcid.org/0000-0002-1646-7866
Elena Puga https://orcid.org/0000-0002-2873-0772
Naseem Rangwala https://orcid.org/0000-0001-9920-7391
Mathias Rapacioli https://orcid.org/0000-0003-2394-6694
Alessandra Ricca https://orcid.org/0000-0002-3141-0630
Julia Roman-Duval https://orcid.org/0000-0001-6326-7069
Joseph Roser https://orcid.org/0000-0002-1806-3494
Evelyne Roueff https://orcid.org/0000-0002-4949-8562
Gaël Rouillé https://orcid.org/0000-0002-4016-1461
Farid Salama https://orcid.org/0000-0002-6064-4401
Dinalva A. Sales https://orcid.org/0000-0002-3496-5711
Karin Sandstrom https://orcid.org/0000-0002-4378-8534
Peter Sarre https://orcid.org/0000-0002-4993-1717
Ella Sciamma-O'Brien https://orcid.org/0000-0002-1883-552X
Kris Sellgren https://orcid.org/0000-0003-0817-2862
Matthew J. Shannon https://orcid.org/0000-0001-5681-5151
Sachindev S. Shenoy https://orcid.org/0000-0003-0281-7383
David Teyssier https://orcid.org/0000-0002-6261-5292
Richard D. Thomas https://orcid.org/0000-0002-9145-6366
Aditya Togi https://orcid.org/0000-0001-5042-3421
Laurent Verstraete https://orcid.org/0000-0003-1037-4121
Adolf N. Witt https://orcid.org/0000-00003-0760-4483
Alwyn Wootten https://orcid.org/0000-0001-7026-6099
Nathalie Ysard https://orcid.org/0000-0003-1037-4121
Henning Zettergren https://orcid.org/0000-0002-2493-4161
Yong Zhang https://orcid.org/0000-0002-1086-7922
Ziwei E. Zhang https://orcid.org/0000-0002-9927-2705
Junfeng Zhen https://orcid.org/0000-0002-3972-5266

References

Abel, N. P., Ferland, G. J., O'Dell, C. R., Shaw, G., & Troland, T. H. 2006, ApJ, 644, 344
Abgrall, H., Le Bourlot, J., Pineau Des Forets, G., et al. 1992, A&A, 253, 525
Agúndez, M., Goicoechea, J. R., Cernicharo, J., Faure, A., & Roueff, E. 2010, ApJ, 713, 662
Alata, I., Cruz-Diaz, G. A., Muñoz Caro, G. M., & Dartois, E. 2014, A&A, 569, A119
Allamandola, L. J., Tielens, A. G. G. M., & Barker, J. R. 1985, ApJL, 290, L25
Allers, K. N., Jaffe, D. T., Lacy, J. H., Draine, B. T., & Richter, M. J. 2005, ApJ, 630, 368
Anderson, L. D., Zavagno, A., Deharveng, L., et al. 2012, A&A, 542, A10
Andree-Labsch, S., Ossenkopf-Okada, V., & Röllig, M. 2017, A&A, 598, A2
Andrews, H., Boersma, C., Werner, M. W., et al. 2015, ApJ, 807, 99
Arab, H., Abergel, A., Habart, E., et al. 2012, A&A, 541, A19
Bakes, E. L. O., & Tielens, A. G. G. M. 1994, ApJ, 427, 822
Balick, B., Gammon, R. H., & Hjellming, R. M. 1974, PASP, 86, 616
Bally, J., O'Dell, C. R., & McCaughrean, M. J. 2000, AJ, 119, 2919
Bauschlicher, C. W., Jr., Boersma, C., Ricca, A., et al. 2010, ApJS, 189, 341
Bauschlicher, C. W., Jr., Ricca, A., Boersma, C., & Allamandola, L. J. 2018, ApJS, 234, 32
Bayet, E., Viti, S., Williams, D., Rawlings, J., & Bell, T. 2009, ApJ, 696, 1466
Bell, T., Roueff, E., Viti, S., & Williams, D. 2006, MNRAS, 371, 1865
Bernard-Salas, J., Habart, E., Arab, H., et al. 2012, A&A, 538, A37
Bernard-Salas, J., Peeters, E., Sloan, G. C., et al. 2009, ApJ, 699, 1541
Bernard-Salas, J., & Tielens, A. G. G. M. 2005, A&A, 431, 523
Berné, O., Cox, N. L. J., Mulas, G., & Joblin, C. 2017, A&A, 605, L1
Berné, O., Joblin, C., Deville, Y., et al. 2007, A&A, 469, 575
Berné, O., Joblin, C., Deville, Y., et al. 2012, Proceedings of the Annual Meeting of the French Society of Astronomy and Astrophysics (SF2A), 6, arXiv:1210.3453
Berné, O., Joblin, C., Fuente, A., & Ménard, F. 2009, A&A, 495, 827
Berné, O., Montillaud, J., & Joblin, C. 2015, A&A, 577, A133
Boersma, C., Bauschlicher, C. W. J., Ricca, J. A., et al. 2014, ApJS, 211, 8
Boersma, C., Bregman, J., & Allamandola, L. J. 2015, ApJ, 806, 121
Boersma, C., Rubin, R. H., & Allamandola, L. J. 2012, ApJ, 753, 168
Bregman, J. D., Allamandola, L. J., Tielens, A. G. G. M., Geballe, T. R., & Witteborn, F. C. 1989, ApJ, 344, 791
Bron, E., Agúndez, M., Goicoechea, J. R., & Cernicharo, J. 2018, arXiv:1801.01547
Bron, E., Le Bourlot, J., & Le Petit, F. 2014, A&A, 569, A100
Bron, E., Le Petit, F., & Le Bourlot, J. 2016, A&A, 588, A27
Burton, M. G., Hollenbach, D. J., & Tielens, A. G. G. M. 1990, ApJ, 365, 620
Burton, M. G., Howe, J. E., Geballe, T. R., & Brand, P. W. J. L. 1998, PASA, 15, 194
Calzetti, D. 2020, NatAs, 4, 437
Cami, J. 2011, in EAS Publ. Ser. 46, PAHs and the Universe: A Symposium to Celebrate the 25th Anniversary of the PAH Hypothesis, ed. C. Joblin & A. G. G. M. Tielens (Paris: EDP Sciences), 117
Candian, A., Kerr, T. H., Song, I.-O., McCombie, J., & Sarre, P. J. 2012, MNRAS, 426, 389
Canin, A., Berné, O., & team, T. P. E. 2021, PDRs4all: Simulation and Data Reduction of JWST NIRCam Imaging of an Extended Bright Source, the Orion Bar, arXiv:2112.03106
Canin, A., Berné, O., & team, T. P. E. 2022, PDRs4all: NIRSpec Simulation of Integral Field Unit Spectroscopy of the Orion Bar Photodissociation Region, arXiv:2201.01092
Cardelli, J. A., Clayton, G. C., & Mathis, J. S. 1989, ApJ, 345, 245
Carlsten, S. G., & Hartigan, P. M. 2018, ApJ, 869, 77
Castellanos, P., Berné, O., Sheffer, Y., Wolfire, M. G., & Tielens, A. G. G. M. 2014, ApJ, 794, 83
Cernicharo, J. 2004, ApJL, 608, L41
Cesarsky, D., Lequeux, J., Abergel, A., et al. 1996, A&A, 315, L305
Cesarsky, D., Lequeux, J., Ryter, C., & Gérin, M. 2000, A&A, 354, L87
Champion, J., Berné, O., Vicente, S., et al. 2017, A&A, 604, A69
Chevance, M., Madden, S., Lebouteiller, V., et al. 2016, A&A, 590, A36
Chuss, D. T., Andersson, B. G., Bally, J., et al. 2019, ApJ, 872, 187
Compiègne, M., Abergel, A., Verstraete, L., et al. 2007, A&A, 471, 205
Compiègne, M., Abergel, A., Verstraete, L., & Habart, E. 2008, A&A, 491, 797
Compiègne, M., Verstraete, L., Jones, A., et al. 2011, A&A, 525, A103
Contreras, C. S., & Salama, F. 2013, ApJS, 208, 6
Cormier, D., Lebouteiller, V., Madden, S., et al. 2012, A&A, 548, A20
Cox, N., Pilleri, P., Berné, O., Cernicharo, J., & Joblin, C. 2015, MNRAS: Letters, 456, L89
Croiset, B. A., Candian, A., Berné, O., & Tielens, A. G. G. M. 2016, A&A, 590, A26
Cuadrado, S., Goicoechea, J. R., Cernicharo, J., et al. 2017, A&A, 603, A124
Cuadrado, S., Goicoechea, J. R., Pilleri, P., et al. 2015, A&A, 575, A82
Cuadrado, S., Salas, P., Goicoechea, J. R., et al. 2019, A&A, 625, L3
Cubick, M., Stutzki, J., Ossenkopf, V., Kramer, C., & Röllig, M. 2008, A&A, 488, 623
Dartois, E., Charon, E., Engrand, C., Pino, T., & Sandt, C. 2020, A&A, 637, A82
Deb, N. C., & Hibbert, A. 2011, A&A, 536, A74
Del Zanna, G., Dere, K. P., Young, P. R., & Landi, E. 2021, ApJ, 909, 38

Désert, F.-X., Boulanger, F., & Puget, J.-L. 1990, A&A, 237, 215
Doney, K. D., Candian, A., Mori, T., Onaka, T., & Tielens, A. G. G. M. 2016, A&A, 586, A65
Draine, B. 2003, ARA&A, 41, 241
Draine, B. T. 1978, ApJS, 36, 595
Draine, B. T., & Li, A. 2007, ApJ, 657, 810
Esplugues, G. B., Cazaux, S., Meijerink, R., Spaans, M., & Caselli, P. 2016, A&A, 591, A52
Fazio, G. G., Kleinmann, D. E., Noyes, R. W., et al. 1974, ApJL, 192, L23
Ferland, G. J., Chatzikos, M., Guzmán, F., et al. 2017, RMxAA, 53, 385
Fitzpatrick, E. L., & Massa, D. 1990, ApJS, 72, 163
Foschino, S., Berné, O., & Joblin, C. 2019, A&A, 632, A84
Fuente, A., Rodrıguez-Franco, A., Garcıa-Burillo, S., Martın-Pintado, J., & Black, J. H. 2003, A&A, 406, 899
Galliano, F., Madden, S. C., Tielens, A. G. G. M., Peeters, E., & Jones, A. P. 2008, ApJ, 679, 310
Gardner, J. P., Mather, J. C., Clampin, M., et al. 2006, SSRv, 123, 485
Gatchell, M., Ameixa, J., Ji, M., et al. 2021, NatCo, 12, 6646
Geballe, T. R., Tielens, A. G. G. M., Allamandola, L. J., Moorhouse, A., & Brand, P. W. J. L. 1989, ApJ, 341, 278
Giard, M., Bernard, J. P., Lacombe, F., Normand, P., & Rouan, D. 1994, A&A, 291, 239
Goicoechea, J. R., Aguado, A., Cuadrado, S., et al. 2021, A&A, 647, A10
Goicoechea, J. R., & Cuadrado, S. 2021, A&A, 647, L7
Goicoechea, J. R., Pety, J., Cuadrado, S., et al. 2016, Natur, 537, 207
Goicoechea, J. R., Teyssier, D., Etxaluze, M., et al. 2015, ApJ, 812, 75
Gorti, U., Dullemond, C., & Hollenbach, D. 2009, ApJ, 705, 1237
Gorti, U., & Hollenbach, D. 2002, ApJ, 573, 215
Gould, R. J., & Salpeter, E. E. 1963, ApJ, 138, 393
Großschedl, J. E., Alves, J., Meingast, S., et al. 2018, A&A, 619, A106
Güdel, M., Briggs, K. R., Montmerle, T., et al. 2008, Sci, 319, 309
Guerra, J. A., Chuss, D. T., Dowell, C. D., et al. 2021, ApJ, 908, 98
Guillard, P., Ogle, P., Emonts, B., et al. 2012, ApJ, 747, 95
Guilloteau, C., Oberlin, T., Berné, O., & Dobigeon, N. 2020a, IEEE Trans. Comput. Imaging, 6, 1362
Guilloteau, C., Oberlin, T., Berné, O., Habart, É., & Dobigeon, N. 2020b, AJ, 160, 28
Guzmán, V., Pety, J., Goicoechea, J. R., Gerin, M., & Roueff, E. 2011, A&A, 534, A49
Guzmán, V. V., Pety, J., Goicoechea, J. R., et al. 2015, ApJL, 800, L33
Habart, E., Abergel, A., Boulanger, F., et al. 2011, A&A, 527, A122
Habart, E., Boulanger, F., Verstraete, L., Walmsley, C. M., & Pineau des Forêts, G. 2004, A&A, 414, 531
Habart, E., Dartois, E., Abergel, A., et al. 2010, A&A, 518, L116
Habart, E., Walmsley, M., Verstraete, L., et al. 2005, SSRv, 119, 71
Habing, H. J. 1968, Bull. Astron. Inst.Netherlands, 19, 421
Hartigan, P., Downes, T., & Isella, A. 2020, ApJL, 902, L1
Helou, G., Malhotra, S., Hollenbach, D. J., Dale, D. A., & Contursi, A. 2001, ApJL, 548, L73
Herrmann, F., Madden, S. C., Nikola, T., et al. 1997, ApJ, 481, 343
Hogerheijde, M. R., Jansen, D. J., & van Dishoeck, E. F. 1995, A&A, 294, 792
Hollenbach, D., & Natta, A. 1995, ApJ, 455, 133
Hollenbach, D. J., & Tielens, A. G. G. M. 1999, RvMP, 71, 173
Hony, S., Van Kerckhoven, C., Peeters, E., et al. 2001, A&A, 370, 1030
Jansen, D. J., Spaans, M., Hogerheijde, M. R., & Van Dishoeck, E. F. 1995, A&A, 303, 541
Joblin, C., Bron, E., Pinto, C., et al. 2018, A&A, 615, A129
Joblin, C., Szczerba, R., Berné, O., & Szyszka, C. 2008, A&A, 490, 189
Joblin, C., & Tielens, A. G. G. M. 2011, PAHs and the Universe (Paris: EDP Sciences)
Joblin, C., Tielens, A. G. G. M., Allamandola, L. J., & Geballe, T. R. 1996a, ApJ, 458, 610
Joblin, C., Tielens, A. G. G. M., Geballe, T. R., & Wooden, D. H. 1996b, ApJL, 460, L119
Jones, A. P., Fanciullo, L., Köhler, M., et al. 2013, A&A, 558, A62
Jones, A. P., & Habart, E. 2015, A&A, 581, A92
Jones, A. P., Köhler, M., Ysard, N., Bocchio, M., & Verstraete, L. 2017, A&A, 602, A46
Juvela, M. 2019, A&A, 622, A79
Kaplan, K. F., Dinerstein, H. L., Oh, H., et al. 2017, ApJ, 838, 152
Kaufman, M. J., Wolfire, M. G., & Hollenbach, D. J. 2006, ApJ, 644, 283
Kaufman, M. J., Wolfire, M. G., Hollenbach, D. J., & Luhman, M. L. 1999, ApJ, 527, 795
Kirsanova, M. S., & Wiebe, D. S. 2019, MNRAS, 486, 2525
Knight, C., Peeters, E., Stock, D. J., Vacca, W. D., & Tielens, A. G. G. M. 2021, ApJ, 918, 8
Knight, C., Peeters, E., Tielens, A. G. G. M., & Vacca, W. D. 2022, MNRAS, 509, 3523
Kounkel, M., Hartmann, L., Loinard, L., et al. 2017, ApJ, 834, 142
Lai, T. S. Y., Smith, J. D. T., Baba, S., Spoon, H. W. W., & Imanishi, M. 2020, ApJ, 905, 55
Le Bourlot, J., Le Petit, F., Pinto, C., Roueff, E., & Roy, F. 2012, A&A, 541, A76
Le Bourlot, J., Pineau Des Forets, G., Roueff, E., & Flower, D. R. 1993, A&A, 267, 233
Le Petit, F., Nehmé, C., Le Bourlot, J., & Roueff, E. 2006, ApJS, 164, 506
Leger, A., & Puget, J. L. 1984, A&A, 500, 279
Leurini, S., Rolffs, R., Thorwirth, S., et al. 2006, A&A, 454, L47
Lis, D. C., & Schilke, P. 2003, ApJL, 597, L145
Luhman, M. L., Jaffe, D. T., Keller, L. D., & Pak, S. 1994, ApJL, 436, L185
Malhotra, S., Kaufman, M., Hollenbach, D., et al. 2001, ApJ, 561, 766
Maltseva, E., Petrignani, A., Candian, A., et al. 2015, ApJ, 814, 23
Maragkoudakis, A., Ivkovich, N., Peeters, E., et al. 2018, MNRAS, 481, 5370
Maragkoudakis, A., Peeters, E., & Ricca, A. 2020, MNRAS, 494, 642
Marconi, A., Testi, L., Natta, A., & Walmsley, C. M. 1998, A&A, 330, 696
Martínez, L., Santoro, G., Merino, P., et al. 2020, NatAs, 4, 97
Mattioda, A. L., Hudgins, D. M., Boersma, C., et al. 2020, ApJS, 251, 22
McKinney, J., Pope, A., Armus, L., et al. 2020, ApJ, 892, 119
Meeus, G., Salyk, C., Bruderer, S., et al. 2013, A&A, 559, A84
Menten, K. M., Reid, M. J., Forbrich, J., & Brunthaler, A. 2007, A&A, 474, 515
Montillaud, J., Joblin, C., & Toublanc, D. 2013, A&A, 552, A15
Mori, T. I., Onaka, T., Sakon, I., et al. 2014, ApJ, 784, 53
Mori, T. I., Sakon, I., Onaka, T., et al. 2012, ApJ, 744, 68
Moutou, C., Sellgren, K., Verstraete, L., & Léger, A. 1999, A&A, 347, 949
Murga, M. S., Kirsanova, M. S., Vasyunin, A. I., & Pavlyuchenkov, Y. N. 2020, MNRAS, 497, 2327
Murga, M. S., Kirsanova, M. S., Wiebe, D. S., & Boley, P. A. 2022, MNRAS, 509, 800
Murga, M. S., Wiebe, D. S., Sivkova, E. E., & Akimkin, V. V. 2019, MNRAS, 488, 965
Nagy, Z., Van der Tak, F. F. S., Ossenkopf, V., et al. 2013, A&A, 550, A96
Naslim, N., Kemper, F., Madden, S. C., et al. 2015, MNRAS, 446, 2490
Natta, A., Walmsley, C. M., & Tielens, A. G. G. M. 1994, ApJ, 428, 209
O'Dell, C. R. 2001, ARA&A, 39, 99
Onaka, T., Mori, T. I., Sakon, I., et al. 2014, ApJ, 780, 114
Ossenkopf, V., Röllig, M., Neufeld, D. A., et al. 2013, A&A, 550, A57
Osterbrock, D. E., & Ferland, G. J. 2006, Astrophysics Of Gas Nebulae and Active Galactic Nuclei (Mill Valley, CA: Univ. Science Books)
Pabst, C., Higgins, R., Goicoechea, J. R., et al. 2019, Natur, 565, 618
Pabst, C. H. M., Goicoechea, J. R., Teyssier, D., et al. 2017, A&A, 606, A29
Pabst, C. H. M., Goicoechea, J. R., Teyssier, D., et al. 2020, A&A, 639, A2
Paladini, R., Umana, G., Veneziani, M., et al. 2012, ApJ, 760, 149
Parker, D. S. N., Zhang, F., Kim, Y. S., et al. 2012, PNAS, 109, 53
Parmar, P. S., Lacy, J. H., & Achtermann, J. M. 1991, ApJL, 372, L25
Parravano, A., Hollenbach, D. J., & McKee, C. F. 2003, ApJ, 584, 797
Peeters, E., Allamandola, L. J., Bauschlicher, C. W. J., et al. 2004a, ApJ, 604, 252
Peeters, E., Bauschlicher, C. W., Jr., Allamandola, L. J., et al. 2017, ApJ, 836, 198
Peeters, E., Hony, S., Van Kerckhoven, C., et al. 2002, A&A, 390, 1089
Peeters, E., Spoon, H. W. W., & Tielens, A. G. G. M. 2004b, ApJ, 613, 986
Peeters, E., Tielens, A. G. G. M., Allamandola, L. J., & Wolfire, M. G. 2012, ApJ, 747, 44
Pellegrini, E. W., Baldwin, J. A., Ferland, G. J., Shaw, G., & Heathcote, S. 2009, ApJ, 693, 285
Pilleri, P., Joblin, C., Boulanger, F., & Onaka, T. 2015, A&A, 577, A16
Pilleri, P., Montillaud, J., Berné, O., & Joblin, C. 2012, A&A, 542, A69
Pilleri, P., Treviño-Morales, S., Fuente, A., et al. 2013, A&A, 554, A87

Pound, M. W., & Wolfire, M. G. 2008, in ASP Conf. Ser. 394, Astronomical Data Analysis Software and Systems XVII, ed. R. W. Argyle, P. S. Bunclark, & J. R. Lewis (San Francisco, CA: ASP), 654
Povich, M. S., Stone, J. M., Churchwell, E., et al. 2007, ApJ, 660, 346
Putaud, T., Michaut, X., Le Petit, F., Roueff, E., & Lis, D. C. 2019, A&A, 632, A8
Rapacioli, M., Calvo, F., Joblin, C., et al. 2006, A&A, 460, 519
Rapacioli, M., Joblin, C., & Boissel, P. 2005, A&A, 429, 193
Reach, W. T., Megeath, S. T., Cohen, M., et al. 2005, PASP, 117, 978
Ricca, A., Bauschlicher, C. W. J., Boersma, C., Tielens, A. G. G. M., & Allamandola, L. J. 2012, ApJ, 754, 75
Rieke, G. H., Wright, G., Böker, T., et al. 2015, PASP, 127, 584
Robberto, M., Gennaro, M., Ubeira Gabellini, M. G., et al. 2020, ApJ, 896, 79
Röllig, M., Abel, N. P., Bell, T., et al. 2007, A&A, 467, 187
Röllig, M., Szczerba, R., Ossenkopf, V., & Glück, C. 2013, A&A, 549, A85
Rosenthal, D., Bertoldi, F., & Drapatz, S. 2000, A&A, 356, 705
Sabbah, H., Bonnamy, A., Papanastasiou, D., et al. 2017, ApJ, 843, 34
Salama, F., Sciamma-O'Brien, E., Contreras, C. S., & Bejaoui, S. 2018, in IAU Symp. 332, Astrochemistry VII: Through the Cosmos from Galaxies to Planets, ed. M. Cunningham, T. Miller, & T. Aikawa (Cambridge: Cambridge Univ. Press), 364
Salgado, F., Berné, O., Adams, J. D., et al. 2016, ApJ, 830, 118
Schirmer, T., Abergel, A., Verstraete, L., et al. 2020, A&A, 639, A144
Schirmer, T., Habart, E., Ysard, N., et al. 2021, A&A, 649, A148
Schirmer, T., Ysard, N., Habart, E., et al. 2022, A&A, submitted
Sciamma-O'Brien, E., & Salama, F. 2020, ApJ, 905, 45
Sellgren, K., Tokunaga, A. T., & Nakada, Y. 1990, ApJ, 349, 120
Sellgren, K., Werner, M. W., Ingalls, J. G., et al. 2010, ApJL, 722, L54
Shannon, M. J., & Boersma, C. 2018, in Proc. 17th Python in Science Conf., ed. F. Akici, 99
Shaw, G., Ferland, G. J., Henney, W. J., et al. 2009, ApJ, 701, 677
Sheffer, Y., Wolfire, M. G., Hollenbach, D. J., Kaufman, M. J., & Cordier, M. 2011, ApJ, 741, 45
Sidhu, A., Peeters, E., Cami, J., & Knight, C. 2021, MNRAS, 500, 177
Simon, R., Stutzki, J., Sternberg, A., & Winnewisser, G. 1997, A&A, 327, L9
Sloan, G. C., Bregman, J. D., Geballe, T. R., Allamandola, L. J., & Woodward, E. 1997, ApJ, 474, 735
Smith, J. D. T., Armus, L., Dale, D. A., et al. 2007, PASP, 119, 1133
Smyth, R. T., Ramsbottom, C. A., Keenan, F. P., Ferland, G. J., & Ballance, C. P. 2019, MNRAS, 483, 654
Stepnik, B., Abergel, A., Bernard, J. P., et al. 2003, A&A, 398, 551
Sternberg, A., & Dalgarno, A. 1989, ApJ, 338, 197
Sternberg, A., & Dalgarno, A. 1995, ApJS, 99, 565
Stock, D. J., Choi, W. D. Y., Moya, L. G. V., et al. 2016, ApJ, 819, 65
Stock, D. J., & Peeters, E. 2017, ApJ, 837, 129
Stoerzer, H., Stutzki, J., & Sternberg, A. 1995, A&A, 296, L9
Störzer, H., & Hollenbach, D. 1998, ApJ, 495, 853
Tabone, B., van Hemert, M. C., van Dishoeck, E. F., & Black, J. H. 2021, A&A, 650, A192
Tauber, J. A., Lis, D. C., Keene, J., Schilke, P., & Buettgenbach, T. H. 1995, A&A, 297, 567
Tauber, J. A., Tielens, A. G. G. M., Meixner, M., & Goldsmith, P. F. 1994, ApJ, 422, 136
Tielens, A. G. G. M. 2005, The Physics and Chemistry of the Interstellar Medium (Cambridge: Cambridge Univ. Press)
Tielens, A. G. G. M., & Hollenbach, D. 1985a, ApJ, 291, 747
Tielens, A. G. G. M., & Hollenbach, D. 1985b, ApJ, 291, 722
Tielens, A. G. G. M., Meixner, M. M., van der Werf, P. P., et al. 1993, Sci, 262, 86
van den Ancker, M. E., Tielens, A. G. G. M., & Wesselius, P. R. 2000, A&A, 358, 1035
van der Tak, F. F. S., Nagy, Z., Ossenkopf, V., et al. 2013, A&A, 560, A95
van der Werf, P. P., Goss, W. M., & O'Dell, C. R. 2013, ApJ, 762, 101
van der Werf, P. P., Stutzki, J., Sternberg, A., & Krabbe, A. 1996, A&A, 313, 633
van Dishoeck, E. F., & Black, J. H. 1986, ApJS, 62, 109
Verma, A., Lutz, D., Sturm, E., et al. 2003, A&A, 403, 829
Verstraete, L., Leger, A., D'Hendecourt, L., Defourneau, D., & Dutuit, O. 1990, A&A, 237, 436
Vicente, S., Berné, O., Tielens, A. G. G. M., et al. 2013, ApJ, 765, L38
Visser, R., Geers, V., Dullemond, C., et al. 2007, A&A, 466, 229
Wakelam, V., Bron, E., Cazaux, S., et al. 2017, MolAs, 9, 1
Walmsley, C., Natta, A., Oliva, E., & Testi, L. 2000, A&A, 364, 301
Watson, C., Povich, M. S., Churchwell, E. B., et al. 2008, ApJ, 681, 1341
Weilbacher, P. M., Monreal-Ibero, A., Kollatschny, W., et al. 2015, A&A, 582, A114
Weingartner, J. C., & Draine, B. T. 2001, ApJS, 134, 263
Wen, Z., & O'dell, C. 1995, ApJ, 438, 784
Werner, M. W., Gatley, I., Harper, D. A., et al. 1976, ApJ, 204, 420
Wiersma, S. D., Candian, A., Bakker, J. M., et al. 2020, A&A, 635, A9
Woitke, P., Kamp, I., & Thi, W.-F. 2009, A&A, 501, 383
Wolfire, M. G., McKee, C. F., Hollenbach, D., & Tielens, A. G. G. M. 2003, ApJ, 587, 278
Wolfire, M. G., Tielens, A. G. G. M., & Hollenbach, D. 1990, ApJ, 358, 116
Wright, C. M., van Dishoeck, E. F., Cox, P., Sidher, S. D., & Kessler, M. F. 1999, ApJL, 515, L29
Wyrowski, F., Schilke, P., Hofner, P., & Walmsley, C. M. 1997, ApJL, 487, L171
Young Owl, R. C., Meixner, M. M., Wolfire, M., Tielens, A. G. G. M., & Tauber, J. 2000, ApJ, 540, 886
Zettergren, H., Domaracka, A., Schlathoelter, T., et al. 2021, EPJD, 75, 152
Zhang, Z. E., Cummings, S. J., Wan, Y., Yang, B., & Stancil, P. C. 2021, ApJ, 912, 116